Zoologica Scripta

KUNGL. VETENSKAPS-AKADEMIEN
THE ROYAL SWEDISH ACADEMY OF SCIENCES

Synergistic effects of combining morphological and molecular data in resolving the phylogenetic position of *Semispathidium* (Ciliophora, Haptoria) with description of *Semispathidium breviarmatum* sp. n. from tropical Africa

Peter Vďačný & Wilhelm Foissner

Submitted: 18 February 2013
Accepted: 24 April 2013
doi:10.1111/zsc.12023

Vd'ačný, P. & Foissner, W. (2013). Synergistic effects of combining morphological and molecular data in resolving the phylogenetic position of *Semispathidium* (Ciliophora, Haptoria) with description of *Semispathidium breviarmatum* sp. n. from tropical Africa. —*Zoologica Scripta*, *42*, 529–549.

We describe a new species, *Semispathidium breviarmatum* sp. n., from tropical Africa and analyse its phylogenetic position within the subclass Haptoria, using live observation, various silver impregnation methods, SEM and the 18S rRNA gene. *Semispathidium breviarmatum* differs from its congeners by the much higher number of ciliary rows and by the shape and size of the extrusomes, that is, extrusive organelles that kill the prey. The phylogenetic position of *Semispathidium* is controversial due to its 'hybrid' morphology. Specifically, the cylindroidal body has a more or less discoidal oral bulge indicating an enchelyodonid origin, while the anteriorly curved somatic kineties suggest a spathidiid ancestor. In order to reconstruct the evolutionary history of *Semispathidium* and to unravel its affinity to other haptorians, we used synergistic effects of combining morphological and molecular data coming from 34 haptorian taxa. These analyses show that *Semispathidium* belongs to the order Spathidiida representing a basal lineage that is far from ordinary *Spathidium* species, but very likely related to *Protospathidium* and *Enchelys*. Any closer phylogenetic relationship between *Semispathidium* and *Enchelyodon* spp. is not recognized in morphological and molecular phylogenies and is consistently excluded by statistical tree topology tests.

Corresponding author: *Peter Vd'ačný*, *Department of Zoology*, *Faculty of Natural Sciences*, *Comenius University*, *Mlynská dolina B-1*, *842 15 Bratislava*, *Slovakia*. *E-mail: vdacny@fns.uniba.sk*

Wilhelm Foissner, *FB Organismische Biologie*, *Universität Salzburg*, *Hellbrunnerstraße 34*, *A-5020*, *Salzburg*, *Austria*. *E-mail: wilhelm.foissner@sbg.ac.at*

Introduction

Many predatory ciliates exhibit a holotrichously ciliated bursiform or spatulate body with anteriorly located oral apparatus carrying toxicysts that are used to overwhelm and kill the prey. This type of ciliates was discovered already 260 years ago by Hill (1752), but the first rapacious genus, *Enchelys*, was legally described about 20 years later by Müller (1773). Subsequent protozoologists, particularly, Dujardin (1841) and Claparède & Lachmann (1859), recognized several further predatory ciliate genera including the well-known *Spathidium* and *Enchelyodon*. These old genera served for a long time as 'collective groups' for various more or less closely related carnivorous ciliates. It was only in the past 30 years that electron microscopy and silver impregnation provided new features for a more reliable morphological characterization and natural classification of this difficult assemblage of ciliates (e.g. Dragesco & Dragesco-Kernéis 1979; Foissner 1984; Foissner & Foissner 1985, 1988; Foissner *et al.* 1995, 1999, 2002; Foissner & Xu 2007). These studies also showed that both the cytoarchitectural diversity and the species diversity of rapacious ciliates are tremendous, as already assumed by Kahl (1930a,b, 1931).

Based on the predatory lifestyle and general morphology, Corliss (1979) assigned *Enchelys*, *Enchelyodon*, *Spathidium* and other rapacious genera to the Haptoria, which now belong to the highly diverse class Litostomatea (Lynn 2008). The higher classification of haptorians has been corroborated by ultrastructural (e.g. Williams *et al.* 1981; Foissner & Foissner 1985, 1988; Lipscomb & Riordan 1990, 1992) and molecular (e.g. Strüder-Kypke *et al.* 2006; Gao *et al.* 2008; Pan *et al.* 2010; Vd'ačný *et al.* 2010, 2011a,b, 2012; Zhang *et al.* 2012) studies. However, the internal phylogenetic relationships among haptorians, as inferred from morphological traits and molecular markers, are rather inconsistent. This is very likely caused by morphological homoplasies and by one or several rapid radiation events, which make reconstruction of the haptorian evolutionary history extremely difficult (Vd'ačný *et al.* 2011a).

In this study, we describe a new species of the genus *Semispathidium*, whose members appear at first glance like *Enchelyodon* while their ciliary pattern resembles that of *Spathidium* (Foissner *et al.* 2002). Thus, it is not clear whether *Semispathidium* is more closely related to *Enchelyodon* or *Spathidium* (Foissner *et al.* 2010). To overcome this problem, we have used cladistic and molecular approaches as well as the synergistic effects of combining morphological and molecular data into a single matrix.

Material and methods

Sample collecting and processing

Samples were collected from terrestrial and semi-terrestrial habitats of tropical Africa in February 1995. A detailed description of the sites and material studied is given in the 'Occurrence and ecology' section. All materials were air-dried for at least one month at room temperature and then were stored in plastic bags until investigation. Ciliates were reactivated from resting cysts using the non-flooded Petri dish method, as described in Vd'ačný & Foissner (2012). This technique involves placing 50–500 g of the air-dried samples in Petri dishes and saturating, but not flooding them, with distilled water. Such Petri dish cultures were analysed for ciliates by inspecting about 2 ml of the soil eluate weekly for a month. For phylogenetic analyses, 18 cells of *Semispathidium breviarmatum* sp. n. (designated '*Semispathidium* sp.' in Vd'ačný *et al.* 2011a, 2012) were collected from the type locality. DNA extraction, amplification and sequencing were described by Vd'ačný *et al.* (2011a, 2012).

Taxonomic methods and terminology

Semispathidium breviarmatum sp. n. was investigated using a combination of *in vivo* observation, silver impregnation and scanning electron microscopy (SEM). Live ciliates and resting cysts were studied at magnifications of 40–1000× with brightfield and differential interference contrast. The ciliature and silverline patterns were revealed with the protargol (protocol A) and the Chatton–Lwoff silver nitrate impregnation methods, respectively (Foissner 1991; Vd'ačný & Foissner 2012). Counts and measurements on protargol-impregnated specimens were conducted at a magnification of 1000×. Statistical analyses were performed with Microsoft Excel for Windows. Formation of resting cysts was induced by isolating several free-swimming cells on slides with a concave deepening containing centrifuged soil eluate. Such preparations were placed in a moist chamber to prevent drying and checked every 24 h until resting cysts were formed. Illustrations of live specimens were based on free-hand sketches and/or micrographs, while those of prepared cells were made with the aid of a drawing device.

Terminology is according to Foissner & Xu (2007). The higher classification of haptorians follows Vd'ačný *et al.* (2011a). By spathidiids, we mean the order Spathidiida as defined by Foissner & Xu (2007). By 'traditional haptorids', we mean taxa that were traditionally classified within the order Haptorida by Foissner & Foissner (1988), but that nest within the order Spathidiida in molecular phylogenies (Vd'ačný *et al.* 2011a). By 'true haptorids', we mean taxa whose traditional and molecular classifications are consistent.

Cladistic analyses

Morphological evolution within the subclass Haptoria and the phylogenetic position of *Semispathidium* were analysed using the computer programs PAUP* ver. 4.0b8 (Swofford 2003) and MrBayes ver. 3.1.2 (Ronquist & Huelsenbeck 2003). The cladistic analyses were based on 27 interphase characteristics that are considered as phylogenetically informative (Table 1). Further, we selected 34 taxa that represent all major haptorian lineages and have 18S rRNA gene sequences deposited in GenBank. All morphological data were obtained from our own observations, original descriptions or authoritative redescriptions (Wenzel 1959; Foissner 1983, 1984; Foissner & Foissner 1985, 1988; Foissner & Leipe 1995; Foissner *et al.* 1995, 1999, 2002; Song *et al.* 2003; Lin *et al.* 2005, 2007, 2008; Foissner & Al-Rasheid 2007; Foissner & Xu 2007; Kim & Min 2009; Pan *et al.* 2010). Cyclotrichiid (*Mesodinium pulex* and *Myrionecta rubra*) and several haptorid (*Chaenea* spp. and *Trachelotractus* spp.) taxa were excluded from the cladistic analyses for reasons explained in the 'Phylogenetic analyses' section. The characters and character states are summarized in Table 1, and their distribution is given in Table 2. Plesiomorphic and apomorphic nature of the character states was discussed by Vd'ačný *et al.* (2010, 2011a,b).

© 2013 The Norwegian Academy of Science and Letters, **42**, 5, September 2013, pp 529–549

Table 1 Characters, character states and coding used for the cladogram shown in Fig. 7

No.	Character	Plesiomorphic	Apomorphic
1	Body shape	Bursiform to cylindroidal (coded 0)	Spatulate (coded 1) Lanceolate (coded 2) Cup-shaped (coded 3)
2	Differentiation of anterior body end	None (coded 0)	Head-like structure (coded 1) Proboscis-like cone (coded 2) Three lobe-like structures (coded 3)
3	Body distinctly dorsoventrally flattened	No (coded 0)	Yes (coded 1)
4	Macronuclear pattern	Mononucleate (coded 0)	Binucleate (coded 1) Moniliform (coded 2) Multinucleate, scattered (coded 3)
5	Number of micronuclei	1 (coded 0)	>1 (coded 1)
6	Number of extrusome types	1 (coded 0)	2 (coded 1)
7	Shape of type I extrusomes	Rod-shaped (coded 0)	Ovate (coded 1) Asymmetrically obclavate (coded 2) Nail-shaped (coded 3)
8	Dorsal warts with extrusomes	Absent (coded 0)	Present (coded 1)
9	Number of contractile vacuoles	1 (coded 0)	2 (coded 1) $\geq$3 (coded 2)
10	Localization of contractile vacuoles	Terminal (coded 0)	Subterminal (coded 1) In a diagonal pattern (coded 2) In a row (coded 3) In a dorsal and ventral row (coded 4)
11	Course of somatic ciliary rows	Meridional (coded 0)	Helical (coded 1)
12	Somatic kineties curved anteriorly	No (coded 0)	Yes (coded 1)
13	Somatic ciliature differentiated into girdles	No (coded 0)	Yes (coded 1)
14	Number of ciliary girdles	1 (coded 0)	2 (coded 1)
15	Right side somatic kineties form a spica in anterior body half	No (coded 0)	Yes (coded 1)
16	Left side somatic kineties form a spica in anterior body half	No (coded 0)	Yes (coded 1)
17	Left side kineties unciliated or bearing stumps	No (coded 0)	Yes (coded 1)
18	Subapical condensation of cilia in one somatic kinety right of dorsal brush	Absent (coded 0)	Present (coded 1)
19	Head kineties	Absent (coded 0)	Present (coded 1)
20	Number of dorsal brush rows	3 (coded 0)	1 (coded 1) 2 (coded 2) 4–5 (coded 3) >5 (coded 4)
21	Localization of dorsal brush	On dorsal side or slightly dorsolaterally (coded 0)	On left side (coded 1) Around the whole body (coded 2) Near ventral side (coded 3)
22	Oral apparatus	Restricted to anterior body pole (coded 0)	Slanted on or extending over ventral side (coded 1)
23	Oral bulge warts	Absent (coded 0)	Present (coded 1)
24	Dikinetidal circumoral kinety	Present (coded 0)	Transformed into perioral kinety 1 and 2 (coded 1) Absent (coded 2)
25	Structure of circumoral kinety	Continuous (coded 0)	Fragmented (coded 1)
26	Oralized somatic kinetids	Absent (coded 0)	Present (coded 1)
27	Perioral kinety 3	Absent (coded 0)	Present (coded 1)

For distribution of character states in the taxa, see Table 2.

The cladograms were computed in a maximum parsimony (MP) framework with unordered states in all characters. In the first set of analyses, all characters were unweighted. This resulted in very poorly resolved cladograms very likely due to the homoplastic nature and/or conflicting signal of several characters. To receive a better statistical support and resolution, character 12 was double-weighted and characters 15, 20, 21 and 27 were triple-weighted, as

Table 2 Distribution of character states in the taxa analysed with the computer programs PAUP* and MrBayes

	Character states[b]					
Taxon[a]	1–5	6–10	11–15	16–20	21–25	26–27
Haptorida						
Enchelyodon sp. 1	000??	??000	000–0	00000	00000	00
Fuscheria sp.	0000?	03000	000–0	00102	00000	10
Fuscheria terricola	00000	03000	000–0	00102	00000	10
Lacrymariida						
Lacrymaria marina	01000	00000	100–0	00014	20000	00
Phialina salinarum	01000	00000	100–0	00014	20000	00
Didiniida						
Didinium nasutum	32001	10000	01110	00003	000??	00
Monodinium sp.	3200?	??000	01100	00003	000??	00
Spathidiida[c]						
Apobryophyllum schmidingeri	20031	12000	010–0	00004	11000	00
Arcuospathidium cultriforme	20001	00000	010–0	00000	01000	00
Arcuospathidium muscorum	20000	00000	010–0	00000	01000	00
Arcuospathidium namibiense	00031	01000	010–0	00000	01000	00
Balantidion pellucidum	00000	00000	010–0	00000	00001	10
Cultellothrix lionotiformis	20000	00000	010–0	00000	11000	00
Enchelyodon sp. 2	00001	10200	000–0	00000	00000	00
Enchelys gasterosteus	00001	00000	010–0	00000	0002–	10
Enchelys polynucleata	00031	00000	010–0	00000	0002–	10
Epispathidium papilliferum	10031	00000	010–0	00000	00100	00
Lagynophrya acuminata	00001	10000	000–0	00000	00000	00
Protospathidium muscicola	00031	01000	010–0	00000	00001	00
Semispathidium breviarmatum	00000	01000	010–0	00000	00000	00
Spathidium spathula	10000	00000	010–0	00000	00000	00
Spathidium stammeri	10001	??000	010–0	00000	00000	00
Teuthophrys trisulca	0300?	00000	010–0	00000	00000	00
Pleurostomatida						
Amphileptus aeschtae	2013?	00023	000–1	01001	01010	00
Amphileptus procerus	20110	00024	000–1	01001	01010	00
Epiphyllum shenzhenense	2012?	10023	000–1	11001	01010	00
Litonotus paracygnus	20110	00001	000–0	01001	01010	01
Litonotus pictus	2012?	00001	000–0	01001	01010	01
Loxophyllum jini	20121	00023	000–0	01001	01010	01
Loxophyllum rostratum	20110	00101	000–0	01001	01010	01
Loxophyllum spirellum	20110	00101	000–0	01001	01010	01
Pseudoamphileptus macrostoma	20110	00024	000–0	01001	31010	00
Siroloxophyllum utriculariae	20110	00012	000–0	01001	01010	01
Incertae sedis						
Homalozoon vermiculare	00121	10023	000–0	01001	00000	00

[a]Classification of taxa follows Vd'ačný *et al.* (2011a).

[b]For characters and character states, see Table 1. A question mark (?) indicates missing data while a dash (–) indicates an inapplicable character.

[c]Including taxa traditionally assigned to haptorids.

they seem to be of a high phylogenetic importance according to the molecular phylogenies. The most parsimonious trees were found by a heuristic search using the computer program PAUP*, whereby trees were optimized by the application of the accelerated transformation (ACCTRAN). The starting trees were established by stepwise addition, further taxa were added randomly, and the tree bisection–reconnection (TBR) branch-swapping algorithm was in effect. A 50% majority-rule consensus tree was calculated from all most parsimonious trees computed during the heuristic analysis, including the bootstrap method with 100 replicates. The reliability of internal branches in the MP cladogram was also assessed by Bremer indices, which were calculated for individual clades by PRAP ver. 2.0b3 (Müller 2004) in combination with PAUP* using parsimony ratcheting with default settings.

Bayesian inference analyses were performed, using the standard discrete model, which is analogous to a JC model except that it has a variable number of states and the symmetric Dirichlet distribution with its alpha parameter fixed

to infinity (Ronquist & Huelsenbeck 2003). The nodal support in the 50% majority-rule consensus tree came from posterior probabilities, using one million generations and trees sampled every 100 generations. The first 25% of sampled trees were considered burn-in trees and were discarded before constructing the consensus tree.

Phylogenetic analyses

To determine whether the genus *Semispathidium* belongs to the enchelyodonids or spathidiids, we analysed an alignment containing the 18S rRNA gene sequences of 34 taxa that were also included in the cladistic analyses. Due to the mutational saturation, cyclotrichiid (*Mesodinium pulex* and *Myrionecta rubra*) and some haptorid (*Chaenea* spp. and *Trachelotractus* spp.) sequences were not included in the phylogenetic analyses, as they caused long branch effects distorting maximum likelihood phylogenies despite selection of the correct evolutionary model (Vd'ačný *et al.* 2011a; Kück *et al.* 2012). All 18S rRNA gene sequences were retrieved from GenBank, and their accession numbers are provided in Fig. 8. Sequences were aligned according to their primary structure using the Mafft ver. 6.240 program that offers various multiple-alignment strategies (Katoh & Toh 2008). For the haptorian sequences, the L-INS-i method was employed with default settings for gap opening and gap extension. Identification of ambiguous and noisy positions of the 18S rRNA gene alignment was achieved with the computer programs G-blocks ver. 0.91b (Castresana 2000; Talavera & Castresana 2007) and Guidance ver. 1.1 (Penn *et al.* 2010a,b), resulting in two masked alignments. The first alignment, in which ambiguously aligned regions were masked using G-blocks, consisted of 1529 characters, while the second alignment, which was masked using Guidance, contained 1549 characters. For both alignments, the GTR + I + Γ evolutionary model was the best fitted model selected by jModeltest ver. 0.1.1 under the Akaike Information Criterion (Guindon & Gascuel 2003; Posada 2008). This model was implemented in MrBayes ver. 3.2.1 (Ronquist & Huelsenbeck 2003) on the CIPRES Portal ver. 1.15 (Miller *et al.* 2009). Two parallel runs with four MCMC chains (one cold and three heated) were run for five million generations with trees saved every 100 generations. The first 12,500 sampled trees were discarded as 'burn-in' prior to constructing a 50% majority-rule consensus tree. The maximum likelihood (ML) analyses of both alignments were also conducted online on the CIPRES Portal using the RAxML algorithm (Stamatakis *et al.* 2008). Maximum parsimony (MP) trees were constructed in PAUP*. The reliability of the internal branches in the ML and MP trees was assessed by the non-parametric bootstrap approach with 1000 replicates and a heuristic search algorithm.

Combined analyses

In addition to the cladistic analyses and molecular phylogenies, we performed a combined Bayesian inference analysis of a matrix containing 18S rRNA gene sequences (G-blocks alignment) and 27 interphase morphological characteristics coming from 34 haptorian taxa. The GTR + I + Γ evolutionary model was fitted to the molecular partition, while the standard discrete model was fitted to the morphological data. The reliability of the branching pattern was assessed by posterior probabilities coming from four chains run for five million generations sampling every 100 generations. The combined data set was also analysed in a maximum parsimony framework with nodal support coming from 1000 bootstrap replicates using heuristic searches in PAUP*. The reliability of internal branches in the MP tree was also assessed by Bremer indices.

Tree topology tests

Opposite to the topology in the unconstrained trees, we tested the monophyletic origin of *Semispathidium breviarmatum* sp. n. and *Enchelyodon* spp. To this end, four constraints were forced on both 18S rRNA gene alignments: (i) monophyly of *Enchelyodon* spp., (ii) sister relationship of *Enchelyodon* sp. 1 and *S. breviarmatum*, (iii) sister relationship of *Enchelyodon* sp. 2 and *S. breviarmatum*, and (iv) monophyly of *Enchelyodon* spp. and *S. breviarmatum*. All other relationships were unspecified. Constrained trees were built in PAUP*, using the ML criterion and a heuristic search with the TBR swapping algorithm and 10 random sequence addition replicates. Consequently, the site-wise likelihoods for all trees were calculated in PAUP* under the substitution evolutionary models with parameters as suggested by jModeltest. The resulting constrained topologies were compared with the best non-constrained topology using the approximately unbiased test (AU), the weighted Shimodaira–Hasegawa test (WSH) and the weighted Kishino–Hasegawa test (WKH) implemented in the CONSEL ver. 0.1j software package (Shimodaira & Hasegawa 2001).

Tracing of character evolution

To unravel the history of character evolution within the subclass Haptoria, we employed the sophisticated computer program Mesquite ver. 2.5 (Maddison & Maddison 2007). This program can calculate, *inter alia*, proportional likelihoods of character states at ancestral nodes, given a phylogenetic tree and a distribution of character states in the observed (terminal) taxa. We used the combined tree shown in Fig. 9 and the character matrix shown in Table 2. To define the directionality in morphological evolutionary pathways, the combined tree was rooted according to the phylogenetic studies of Vd'ačný *et al.* (2010, 2011a,b). Thus, the root was placed within the branch

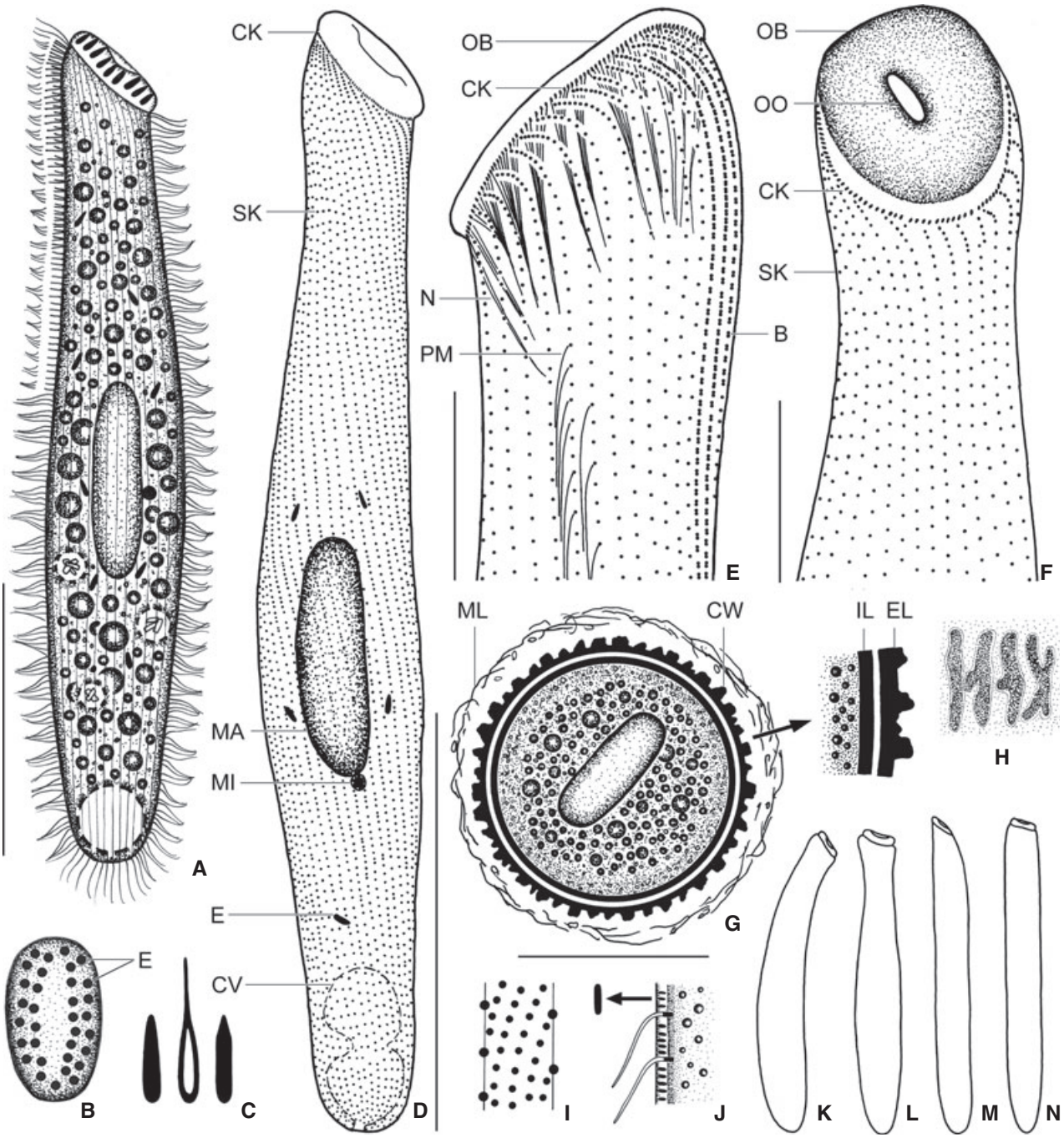

Fig. 1 *Semispathidium breviarmatum* sp. n., type population from life (A–C, G–N) and after protargol impregnation (D–F). —A. Right side view of a representative specimen, length 300 μm. —B. Frontal view of oral bulge showing the extrusomes arranged in two indistinct rings. —C. The oral bulge extrusomes are usually narrowly ovate, rarely thickly needle-shaped, and about 5–7 × 1.3 μm in size. When exploded they display the typical toxicyst structure, i.e., a tube emerging from an empty capsule. —D. Ciliary pattern of right side and nuclear apparatus of holotype specimen, length 270 μm. —E. Left side view of anterior body region of holotype specimen. —F. Ventral view of anterior body region of a paratype specimen. —G. Resting cysts are about 66 μm across and covered by a mucous layer. Arrow denotes a detail of the cyst wall that is composed of two distinct, refractive layers separated by a sheet of lower refractivity. —H. Surface view of resting cyst, showing the rugose pattern. —I, J. Surface view and optical section showing the cortical granulation. The cortical granules are oblong and about 0.5 × 0.2 μm in size. —K–N. Shape variants. B, dorsal brush; CK, circumoral kinety; CV, contractile vacuole; CW, cyst wall; E, extrusomes; EL, external layer; IL, internal layer; MA, macronucleus; MI, micronucleus; ML, mucous layer; N, nematodesmata bundles; OB, oral bulge; OO, oral opening; PM, postciliary microtubules; SK, somatic kineties. Scale bars 20 μm (E, F), 50 μm (G), and 100 μm (A, D).

© 2013 The Norwegian Academy of Science and Letters, **42**, 5, September 2013, pp 529–549

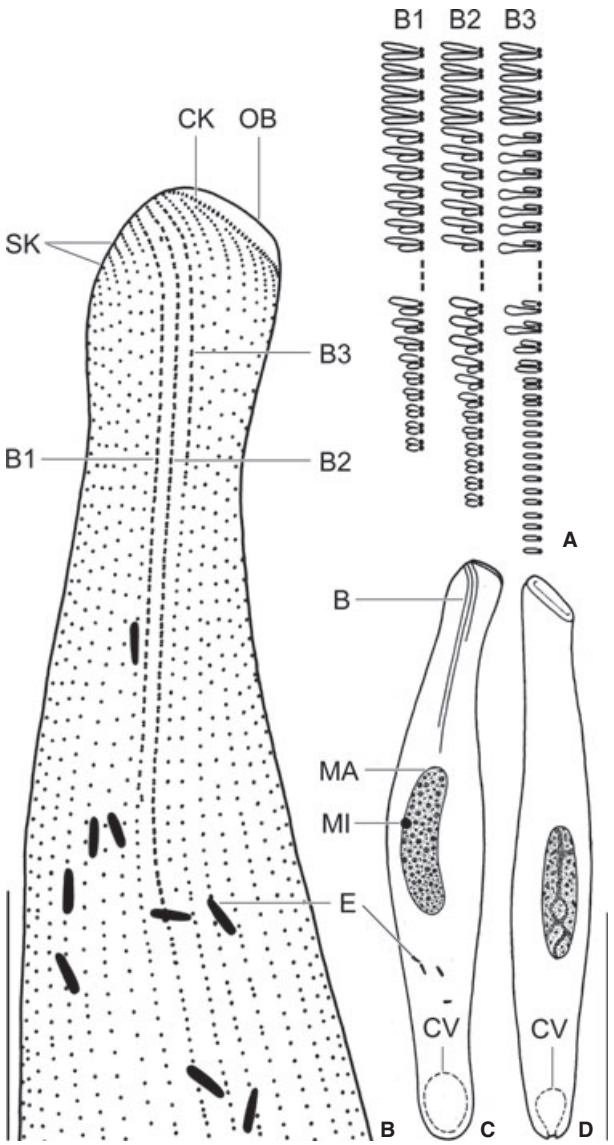

Fig. 2 *Semispathidium breviarmatum* sp. n., type population after protargol impregnation (B–D) and in the scanning electron microscope (A). —A. Dorsal brush, slightly schematized. —B. Dorsal view of ciliary pattern in anterior body half, showing the heterostichad dorsal brush rows. —C, D. Shape variants. B1–3, dorsal brush rows; CK, circumoral kinety; CV, contractile vacuole; E, extrusomes; MA, macronucleus; MI, micronucleus; OB, oral bulge; SK, somatic kineties. Scale bars 30 μm (B) and 100 μm (C, D).

connecting the last common ancestor of the spathidiids and that of the remaining haptorians, that is, as shown in Fig. 9.

Reconstruction of ancestral states was performed with the likelihood method which finds, for each node, the state assignment that maximizes the probability of arriving at the observed states in the terminal taxa (Schulter *et al.* 1997). The evolutionary model used for this likelihood analysis included the Markov k-state 1-parameter model in which the single parameter is the rate of change and any particular change from one state to another is equally probable (Schulter *et al.* 1997; Pagel 1999).

Results

Description of Semispathidium breviarmatum Foissner & Vd'ačný sp. n.

Class Litostomatea Small & Lynn, 1981
Subclass Haptoria Corliss, 1974
Order Spathidiida Foissner & Foissner, 1988;
Family Spathidiidae Kahl in Doflein & Reichenow, 1929
Genus Semispathidium Foissner, Agatha & Berger, 2002;
Semispathidium breviarmatum sp. n. (Figs 1–6; Table 3)
Semispathidium sp. – Vd'ačný et al. 2011a: 512 (18S rRNA gene sequence); Vd'ačný et al. 2012: 398 (ITS1-5.8S rRNA-ITS2 region sequence).

Type material. One holotype and one paratype slide containing protargol-impregnated specimens have been deposited in the Biologiezentrum of the Oberösterreichische Landesmuseum in Linz (LI), Austria. The holotype specimen (Fig. 1D, E) and several relevant paratype specimens have been marked with black ink circles on the coverslip.

Gene sequences. The 18S rRNA gene and the ITS1-5.8S rRNA-ITS2 region nucleotide sequences, both obtained from specimens of the type population, have been deposited in GenBank (http://www.ncbi.nlm.nih.gov/nucleotide/) under accession numbers JF263450 and JX070873, respectively. The 18S rRNA gene sequence is 1641 nucleotides long and has a GC content of 43.4% (Vd'ačný *et al.* 2011a). The ITS1-5.8S rRNA-ITS2 region gene sequence is 368 nucleotides long and has a GC content of 36.7% (Vd'ačný *et al.* 2012).

Diagnosis. Size about 300 × 50 μm *in vivo*. Shape narrowly to very narrowly cylindroidal with distinctly oblique oral bulge. Macronucleus narrowly to very narrowly ellipsoidal; one micronucleus. Oral bulge extrusomes narrowly to very narrowly ovate, about 5–7 × 1–1.3 μm in size, arranged in two indistinct rings. On average 34 ciliary rows, three anteriorly differentiated into a distinctly heterostichad dorsal brush with longest row 2 occupying an average of 36% of body length.

Type locality. Floodplain soil from the Matjulu River in the surroundings of the Berg-en-dal Lodge near the southern border of the Krüger National Park, Republic of South Africa, S25°20′ E31°28′.

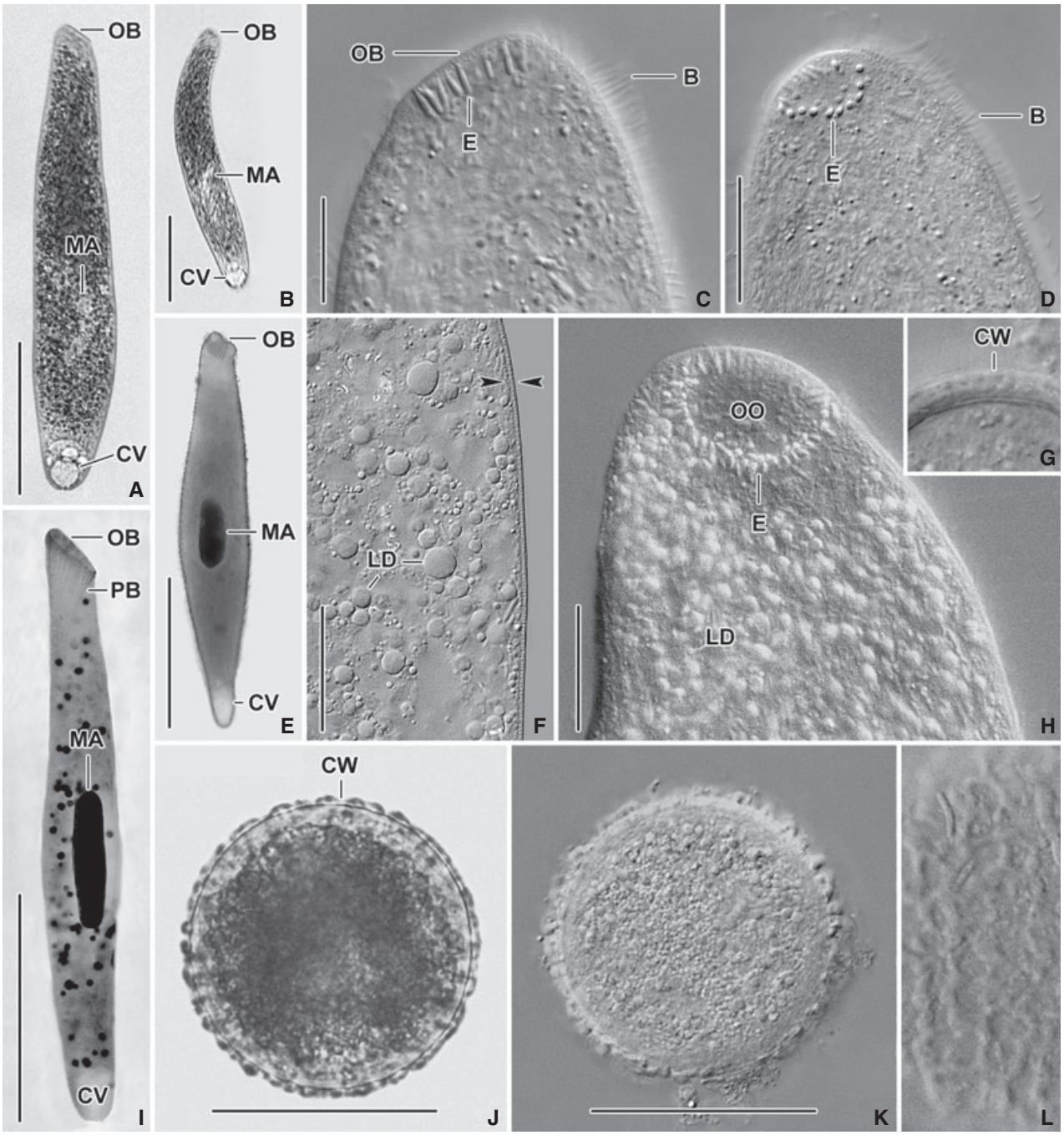

Fig. 3 *Semispathidium breviarmatum* sp. n., type population from life (A–D, F–H, J–L) and after protargol impregnation (E, I). —A, B. Freely motile specimens, showing the slender body, the nuclear and contractile vacuole apparatus, and the cytoplasm packed with globular food (lipid?) inclusions. —C, D, H. Details of anterior body region of slightly squashed specimens, showing the narrowly ovate extrusomes attached to the oral bulge in a ring-shaped pattern. —E, I. Optical sections showing the slender body, the macronucleus, and the contractile vacuole. Note deeply impregnated lipid droplets (I). —F. Optical section showing the cortex (marked by opposed arrowheads) and the 0.5–3 μm-sized lipid droplets. —G. Optical section showing the 4–5 μm-thick cyst wall. —J, K, L. Resting cysts are about 66 μm in diameter and lack an escape apparatus. They display a conspicuous wall with a rugose surface (L). B, dorsal brush; CV, contractile vacuole; CW, cyst wall; E, extrusomes; LD, lipid droplets; MA, macronucleus; OB, oral bulge; OO, oral opening; PB, pharyngeal basket. Scale bars 10 μm (F), 20 μm (C, D, H), 50 μm (J, K), and 100 μm (A, B, E, I).

Table 3 Morphometric data on *Semispathidium breviarmatum* sp. n.

Characteristics[a]	Mean	M	SD	SE	CV	Min	Max	*n*
Body, length (μm)	257.8	250.0	34.2	7.9	13.3	190.0	330.0	19
Body, width (μm)	45.2	44.0	8.7	2.0	19.2	34.0	66.0	19
Body length/width ratio	5.9	5.8	1.2	0.3	20.2	3.6	7.6	19
Oral bulge, length (μm)	22.2	23.0	3.6	0.8	16.4	17.0	29.0	19
Oral bulge, height (μm)	5.5	5.0	0.7	0.2	12.7	4.0	7.0	19
Anterior body end to macronucleus, distance (μm)	109.9	110.0	25.7	5.9	23.4	65.0	180.0	19
Macronucleus, length (μm)	61.8	60.0	8.5	1.9	13.7	48.0	78.0	19
Macronucleus, width (μm)	15.4	15.0	1.6	0.4	10.4	13.0	20.0	19
Micronucleus, length (μm)	4.6	5.0	–	–	–	4.0	5.0	15
Micronucleus, width (μm)	4.6	5.0	–	–	–	4.0	5.0	15
Micronucleus, number	1.0	1.0	0.0	0.0	0.0	1.0	1.0	15
Circumoral kinety to end of brush row 1, distance (μm)	80.4	80.0	7.9	1.8	9.8	65.0	100.0	19
Circumoral kinety to end of brush row 2, distance (μm)	91.4	90.0	9.1	2.1	10.0	76.0	110.0	19
Circumoral kinety to end of brush row 3, distance (μm)	32.5	32.0	3.0	0.7	9.4	25.0	39.0	19
Dikinetids in brush row 1, number	72.8	73.0	13.5	3.1	18.5	52.0	102.0	19
Dikinetids in brush row 2, number	89.7	91.0	16.5	3.8	18.4	65.0	135.0	19
Dikinetids in brush row 3, number	30.8	30.0	3.3	0.8	10.7	24.0	39.0	19
Dorsal brush rows, number	3.0	3.0	0.0	0.0	0.0	3.0	3.0	19
Dorsal brush,% of body length	35.9	34.9	4.8	1.1	13.4	28.8	50.0	19
Dorsal brush rows, maximum length difference in %	64.3	63.4	3.1	0.7	4.9	57.9	69.1	19
Ciliary rows, number in mid-body	33.9	34.0	1.6	0.4	4.7	31.0	37.0	19
Ciliated kinetids in a ventral kinety, number	152.9	140.0	43.1	9.9	28.2	105.0	255.0	19
External oral basket, length (μm)	37.3	35.0	6.2	1.4	16.6	30.0	50.0	19
Cytoplasmic extrusomes, length (μm)	5.4	5.0	–	–	–	5.0	6.0	19

CV, coefficient of variation (%); M, median; Max, maximum; Mean, arithmetic mean; Min, minimum; *n*, number of individuals investigated; SD, standard deviation; SE, standard error of arithmetic mean.

[a]Data based on mounted, protargol-impregnated (Foissner's method), and randomly selected specimens from a non-flooded Petri dish culture.

Etymology. The species-group name *breviarmatum* is a composite of the stem of the Latin adjective *brev·is*, *-is*, *-e* [m, f, n] (short, small, little), the thematic vowel *·i-*, and the Latin adjective *armat·us*, *-a*, *-um* [m, f, n] (armed, armoured), referring to the short extrusomes, a main distinguishing feature of this species.

Description (type population). Size 220–490 × 40–90 μm *in vivo*, usually near 300 × 50 μm as calculated from some *in vivo* measurements and the morphometric data including 15% preparation shrinkage (Table 3); in out of 65 protargol-impregnated cells, two monsters with a size of up to 450 × 55 μm. Shape narrowly to very narrowly ellipsoidal with a length/width ratio of 3.6–7.6:1 *in vivo* and in protargol preparations; body and oral region slightly flattened laterally; anterior body end typically distinctly inclined ventrally, more or less narrowing, sometimes with slightly projecting bulge base; posterior body end narrowly rounded; opisthe postdividers flask-shaped (Figs 1A, D, K–N, 2C, D, 3A, B, E, I and 5A). Nuclear apparatus usually in posterior half of body while dislocated to anterior and rear body third in monster cells and to anterior body half in opisthe postdividers. Macronucleus narrowly ellipsoidal, sometimes slightly curved, about 60 × 15 μm in size after protargol impregnation; nucleoli numerous, globular to irregular, usually 0.2–3 μm across after protargol impregnation, sometimes fusing into oblong masses or forming a reticulate pattern. Micronucleus near by or attached to macronucleus at varying positions, 4–5 μm across; sometimes surrounded by a distinct membrane after protargol impregnation (Figs 1A, D, 2C, D, 3A, B, E, I and 4G; Table 3). Contractile vacuole in rear body end, with several excretory pores in pole area (Figs 1A, D, 2C, D and 3A, B, E, I). Extrusomes scattered throughout cytoplasm and attached to oral bulge forming two indistinct rings; narrowly to very narrowly ovate, rarely thickly acicular, about 5–7 × 1–1.3 μm in size; oral bulge (= mature) extrusomes do not impregnate, while cytoplasmic ones usually impregnate heavily with the protargol method used; exploded extrusomes with typical toxicyst structure, that is, with a tube emerging from an empty capsule (Figs 1B–D, 2B, C, 3C, D, H and 4A–E, G). Cortex very flexible, conspicuous *in vivo* because sharply separated from cytoplasm by tela corticalis; contains about four oblique granule rows between each two kineties; granules loosely spaced, oblong and comparatively small, that is, 0.5 × 0.2 μm (Figs 1I, J and 3F, opposed arrowheads). Protargol-impregnated specimens covered by a 3-μm-thick slime layer (extruded

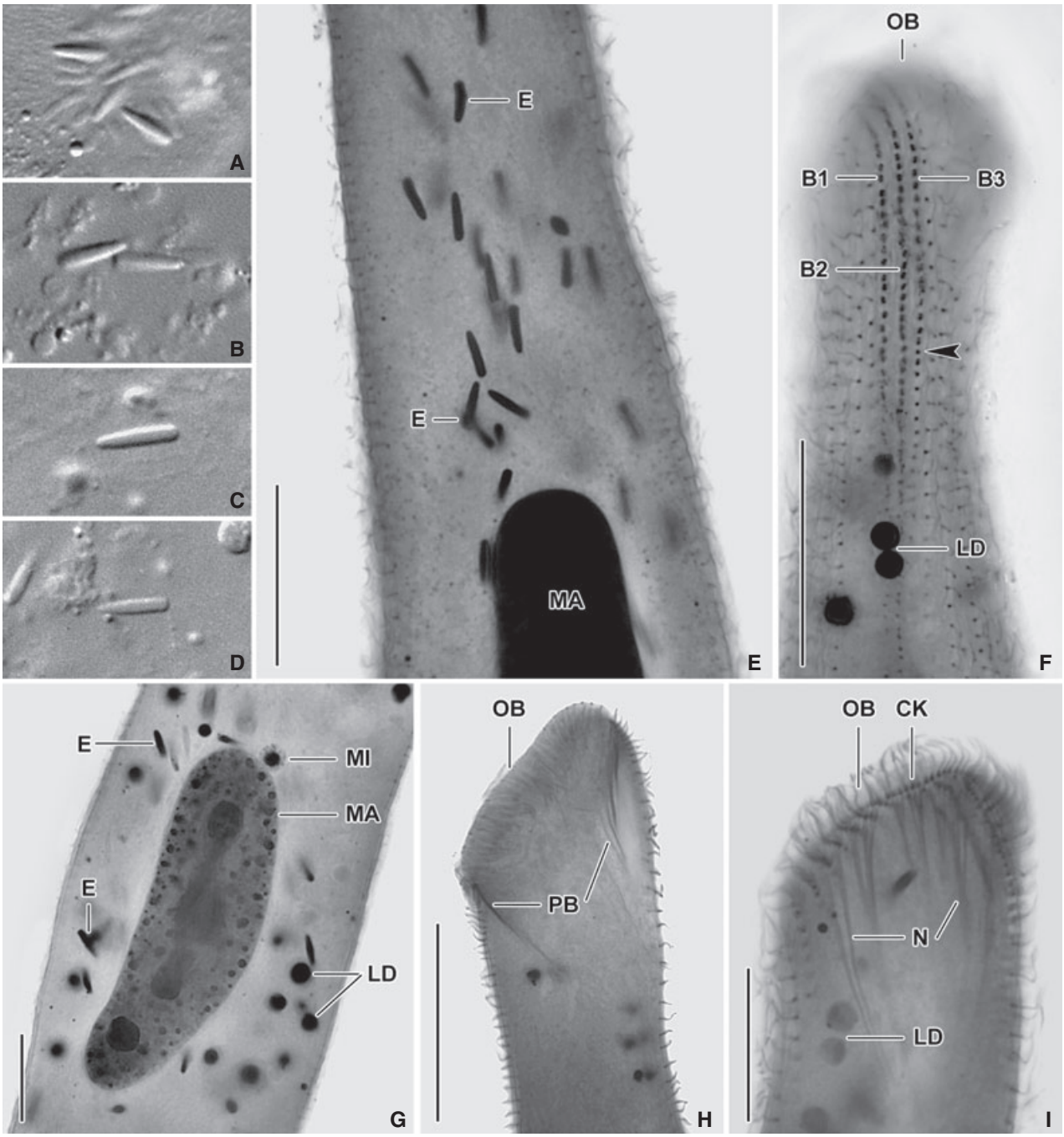

Fig. 4 *Semispathidium breviarmatum* sp. n., type population from life (A–D) and after protargol impregnation (E–I). —A–D. The oral bulge extrusomes are usually narrowly ovate (A–C), rarely thickly needle-shaped (D), and about 5–7 × 1–1.3 μm in size. —E, G. Optical sections showing the deeply impregnated cytoplasmic extrusomes, which are 4–5 μm long, and the nuclear apparatus. The macronuclear nucleoli are numerous, globular to irregular, and sometimes fuse into elongate masses (G). The micronucleus is surrounded by a distinct membrane (G). —F. Dorsal view of ciliary pattern in anterior body region, showing the three-rowed dorsal brush. Arrowhead marks a monokinetid between two brush dikinetids. —H, I. Details of anterior body region, showing the pharyngeal basket made from nematodesmata originating from the circumoral dikinetids. The ciliary rows are distinctly curved anteriorly abutting on the circumoral kinety. B1–3, dorsal brush rows; CK, circumoral kinety; E, extrusomes; LD, lipid droplets; MA, macronucleus; MI, micronucleus; N, nematodesmata; OB, oral bulge; PB, pharyngeal basket. Scale bars 20 μm.

© 2013 The Norwegian Academy of Science and Letters, **42**, 5, September 2013, pp 529–549

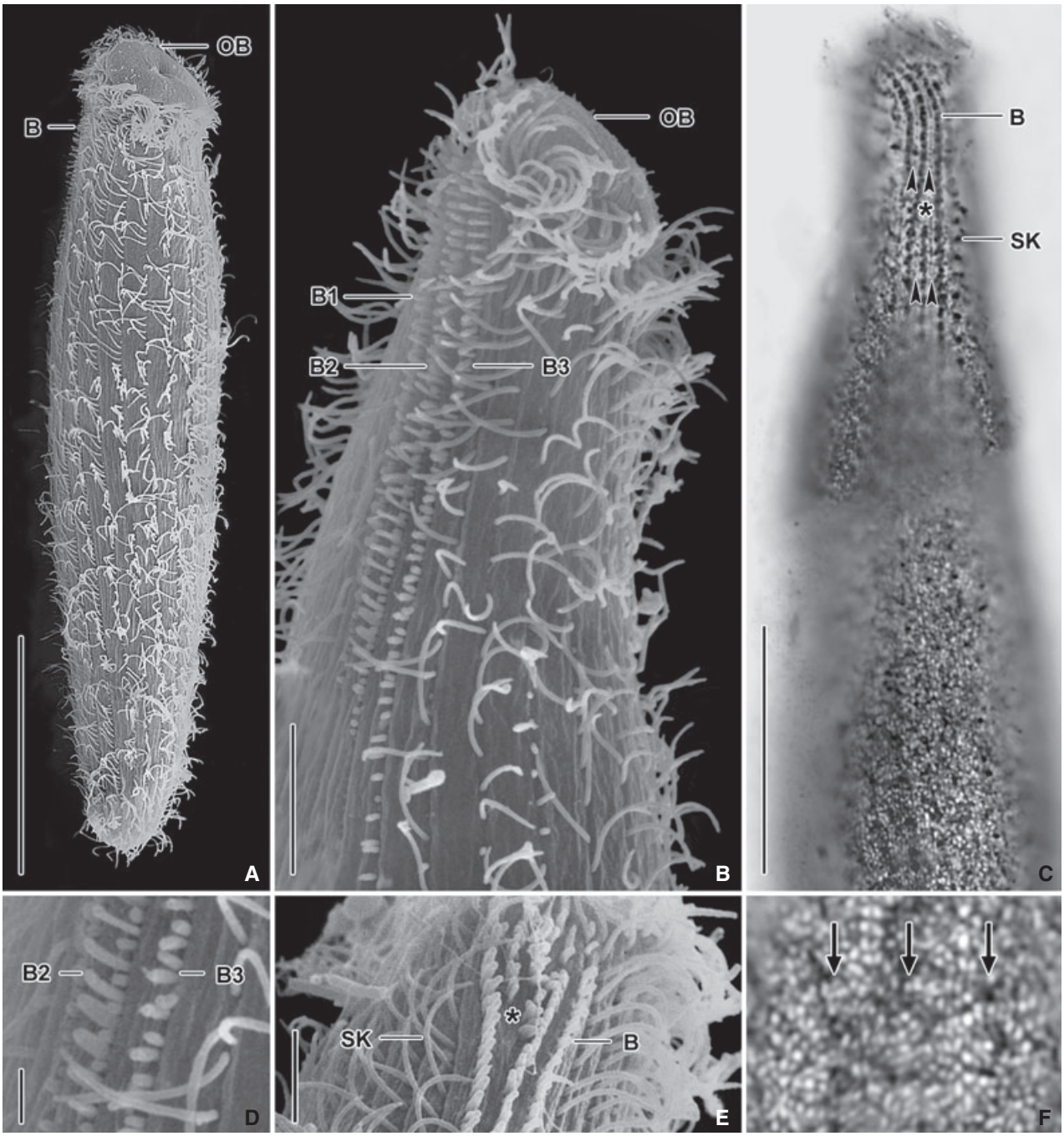

Fig. 5 *Semispathidium breviarmatum* sp. n., type population in the scanning electron microscope (A, B, D, E) and after Chatton-Lwoff silver nitrate impregnation (C, F). —A. Right side view showing the slender body with distinctly oblique oral bulge. —B. Dorsolateral view of anterior body region, showing the tree-rowed dorsal brush and the oblique oral bulge. The narrowly spaced oral cilia form beautiful metachronal waves. —C, F. The silverline pattern is very narrowly and polygonally meshed. The individual meshes are about 0.5–1 μm in size, except between the dorsal brush rows, where they become about 2 μm in size, quadrangular, and divided by a median silverline (arrowheads), and thus forming a platyophryid pattern. Asterisk in (C) marks an extra, anteriorly shortened dorsal brush row extending between rows 2 and 3. Arrows in (F) denote ciliary rows. —D. Detail of posterior brush region of the specimen shown in (B). —E. Dorsal view of anterior body region, showing a malformed dorsal brush with some short additional rows (asterisk). B1–3, dorsal brush rows; OB, oral bulge; SK, somatic kineties. Scale bars 2 μm (D), 5 μm (E), 10 μm (B), and 50 μm (A, C).

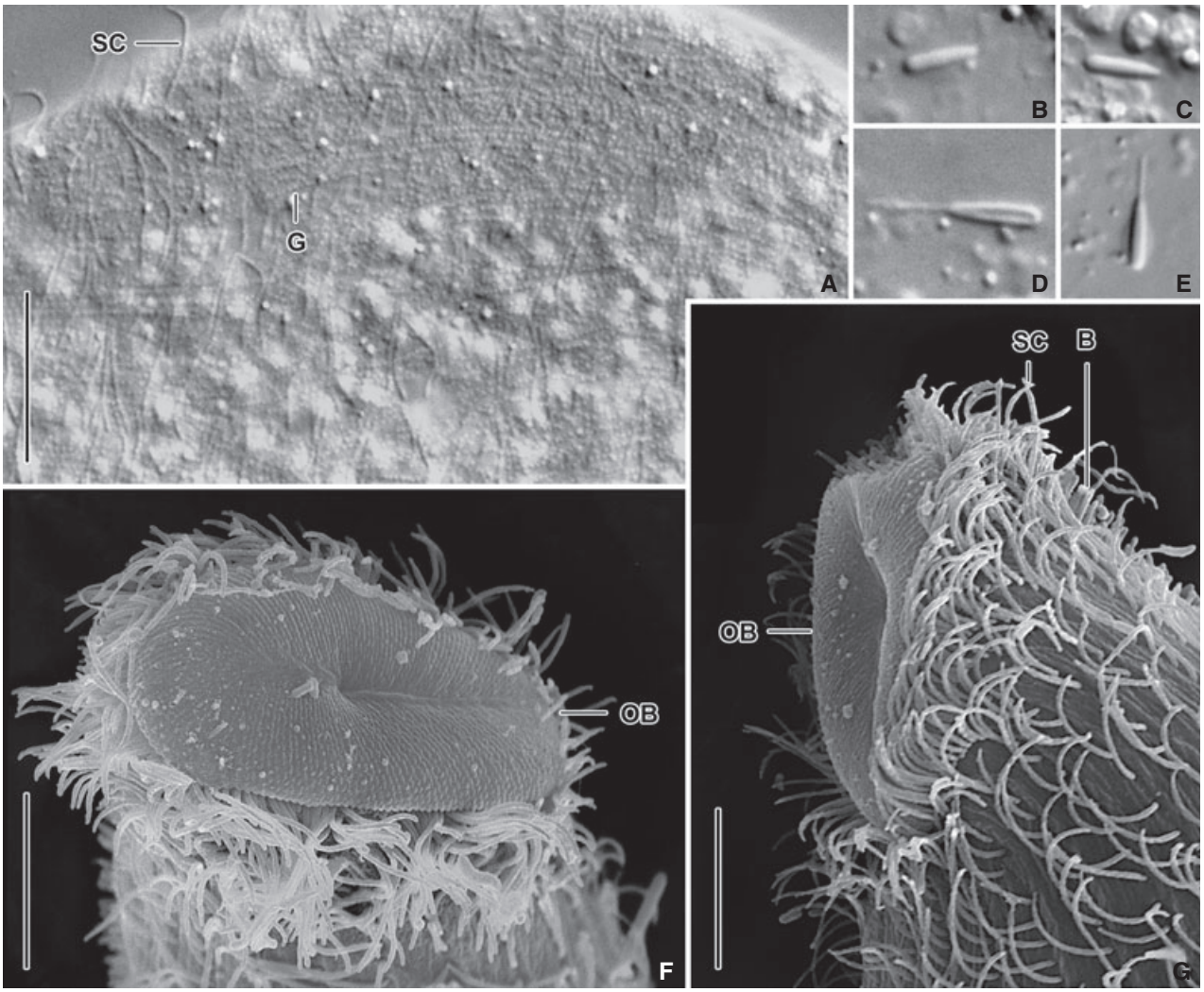

Fig. 6 *Semispathidium breviarmatum* sp. n., type (F, G) and Botswanan (A–E) population from life (A–E) and in the scanning electron microscope (F, G). —A. Surface view showing the dense cortical granulation. —B, C. The oral bulge extrusomes are very narrowly ovate or thickly acicular (C) and have a size of 4–5 × 1 μm. —D, E. Exploded extrusomes show the typical toxicyst structure, i.e., a tube emerging from a capsule. —F. Fronto-lateral view showing the elliptical oral bulge which is transversely striated by fibre bundles very likely originating from the circumoral dikinetids. Densely spaced cilia surround the oral bulge. —G. Left side view of anterior body region, showing the anteriorly curved ciliary rows. B, dorsal brush; G, cortical granules; SC, somatic cilia; OB, oral bulge. Scale bars 10 μm (F, G) and 20 μm (A).

cortical granules?) not recognizable either *in vivo* or in SEM micrographs. Cytoplasm colourless, packed with 0.5–10-μm-sized lipid droplets, some deeply impregnating with the protargol method used; extrusomes; and some globules with crystals possibly coming from hypotrichous prey (Figs 3A, B, I and 4E–G). Swims moderately rapidly by rotating about main body axis, does not glide, shows great flexibility when wriggling between soil particles and curving around obstacles.

Somatic cilia about 10 μm long *in vivo*; spaced ordinarily to narrowly except for about five very densely spaced cilia in curved anterior kinety portion; basal bodies associated with conspicuous (postciliary?) fibres obliquely extending backwards on right side of kineties (Fig. 1E). On average 34 equidistant, narrowly to ordinarily spaced meridional ciliary rows anteriorly curved dorsally on right side of cell while ventrally on left; some rows shortened anteriorly or posteriorly and/or with short breaks; anterior kinety portion only slightly curved in opisthe postdividers (Figs 1D–F, 2B, 4I, 5A, B and 6G; Table 3). Dorsal brush inconspicuous because bristles only up to 4 μm long *in vivo*, becoming 2–3 μm long in protargol preparations and

© 2013 The Norwegian Academy of Science and Letters, **42**, 5, September 2013, pp 529–549

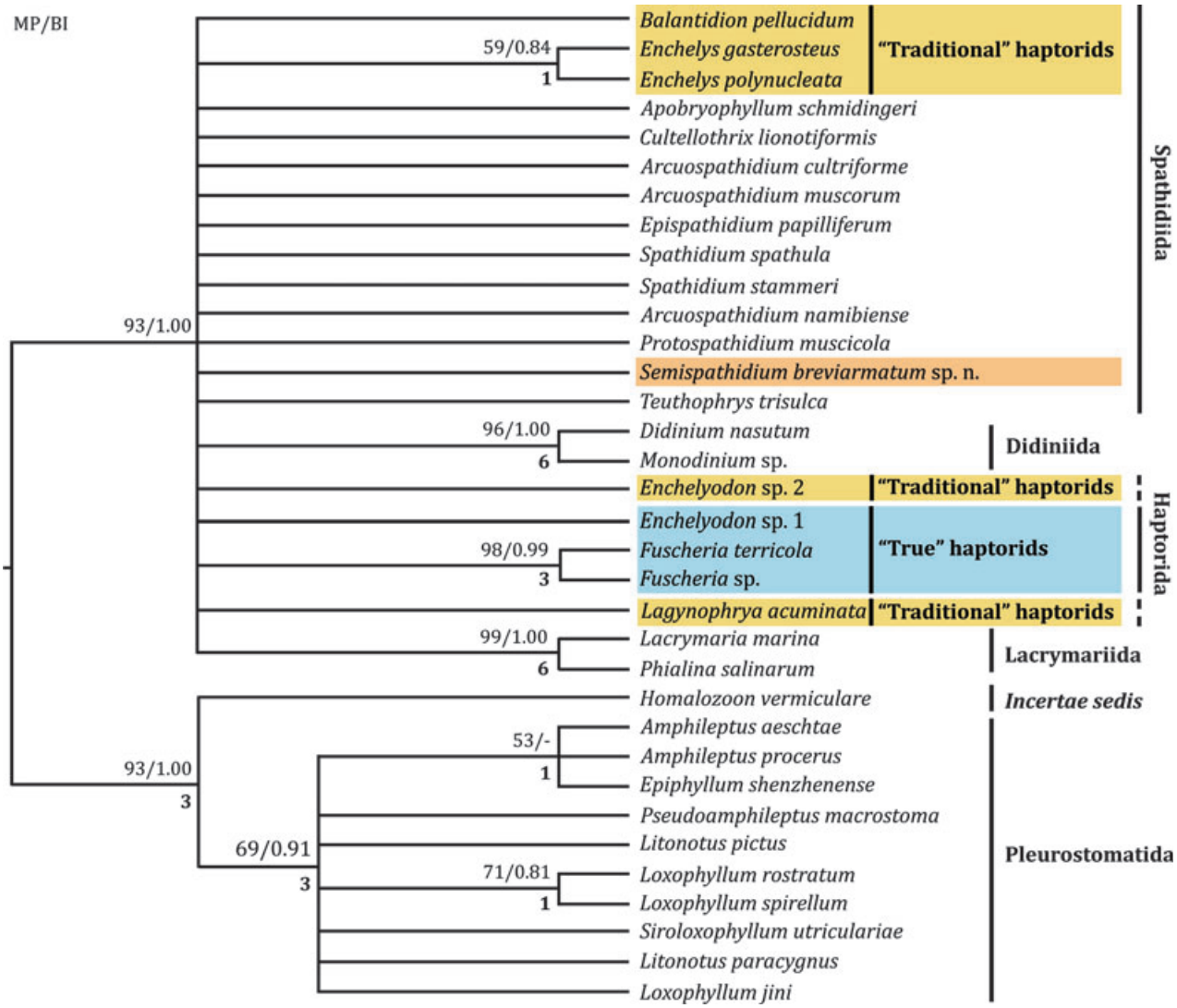

Fig. 7 Fifty percentage majority-rule consensus tree (length = 94, retention index = 0.86, rescaled consistency index = 0.59) inferred from 27 characters of 34 haptorian taxa. The tree was computed with the maximum parsimony analysis implemented in PAUP*. Nodal supports are indicated by bootstrap values for the maximum parsimony (MP) analysis and by posterior probabilities for the Bayesian inference (BI) shown above the nodes. Bremer indices are provided in bold face below the nodes. A dash indicates posterior probabilities below 0.50 for the Bayesian inference.

in SEM micrographs; three-rowed; distinctly heterostichad, that is, length difference between shortest and longest rows 64% on average; in some specimens, heteromorphic in posterior region, especially, in rows 1 and 2 where dikinetids are mixed with monokinetids; often with irregularities, such as breaks or some extra dikinetids forming short additional rows (Figs 4F and 5C, E, asterisks). All brush rows commence with a distinct anterior tail of four to eight monokinetids bearing ordinary cilia and forming curved kinetofragments abutting on circumoral kinety. Brush row 1 slightly shorter than row 2, composed of an average of 73 dikinetids (SEM observations and measurements): anterior bristles more or less distinctly inflated and gradually decreasing in length from about 1.3–2.7 μm to 0.6–1.2 μm, posterior bristles as long as anterior ones in proximal and distal brush portions, while about one half to one-third of anterior bristle length in middle brush portion. Brush row 2 longest and occupying about 36% of body length on average, composed of about 90 dikinetids associated with bristles similar to those of row 1. Brush row 3 distinctly shorter than rows 1 and 2, composed of an average of 31 dikinetids (SEM observations and measurements): anterior portion of row with both bristles more or less inflated and 1.8–3 μm long, middle portion with

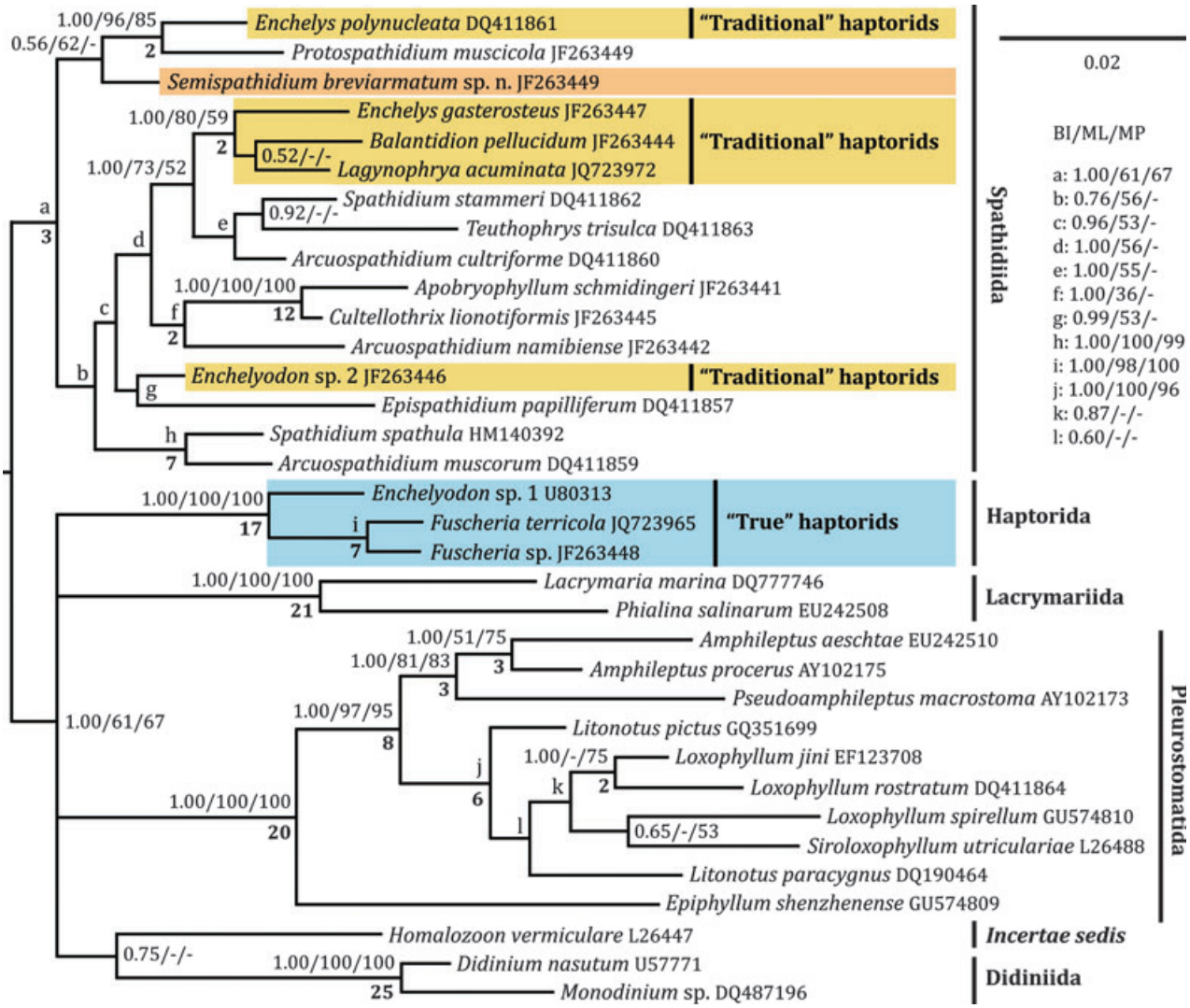

Fig. 8 Small subunit rRNA gene phylogeny based on 1529 nucleotide characters (G-blocks alignment) from 34 haptorian taxa. The tree was constructed using three methods (Bayesian inference, maximum likelihood, and maximum parsimony) with the GTR + I + Γ evolutionary model and the gamma shape parameter at 0.4320, the proportion of invariable sites at 0.6320, and a rate matrix for the model as suggested by jModeltest. Posterior probabilities for the Bayesian inference (BI) and bootstrap values for maximum-likelihood (ML) and maximum-parsimony (MP) are shown above the nodes. Bremer indices are provided in bold face below the nodes. A dash indicates ML and/or MP bootstraps below 50%. The scale bar indicates two substitutions per one hundred nucleotide positions.

stump-like, 0.6- to 0.9-μm-long anterior bristles and clavate, 2.2- to 3-μm-long posterior bristles gradually decreasing to 1.2–1.8 μm in posterior brush portion. Monokinetidal tail of brush row 3 extends to mid-body with 1.2–1.4 μm long bristles in SEM micrographs. Brush dikinetids ordinarily to widely spaced; anterior basal body sometimes appears slightly smaller than posterior one in protargol preparations (Figs 1E, 2A, B, 4F and 5A–E; Table 3).

Silverline pattern as typical for spathidiids, that is, very narrowly and polygonally meshed. Individual meshes about 0.5–1 μm in size, except between dorsal brush rows, where meshes become larger (~ 2 μm in size), quadrangular and divided by a median silverline, forming a platyophryid pattern (Fig. 5C, F).

Oral bulge occupies slightly to ordinarily oblique anterior body end (20–55°, mean = 38°, n = 7); conspicuous because rather distinctly set off from body proper and 4–7 μm high; broadly elliptical in frontal view and about 20–25 × 13–14 μm in SEM micrographs; flat with concave central area; dotted by extrusome tips and transversely striated by fibre bundles very likely originating from circumoral dikinetids (Figs 1A, B, D, F, K–N, 5A, B and 6F, G; Table 3). Circumoral kinety at base of oral bulge and of same shape, composed of narrowly spaced dikinetids

© 2013 The Norwegian Academy of Science and Letters, **42**, 5, September 2013, pp 529–549

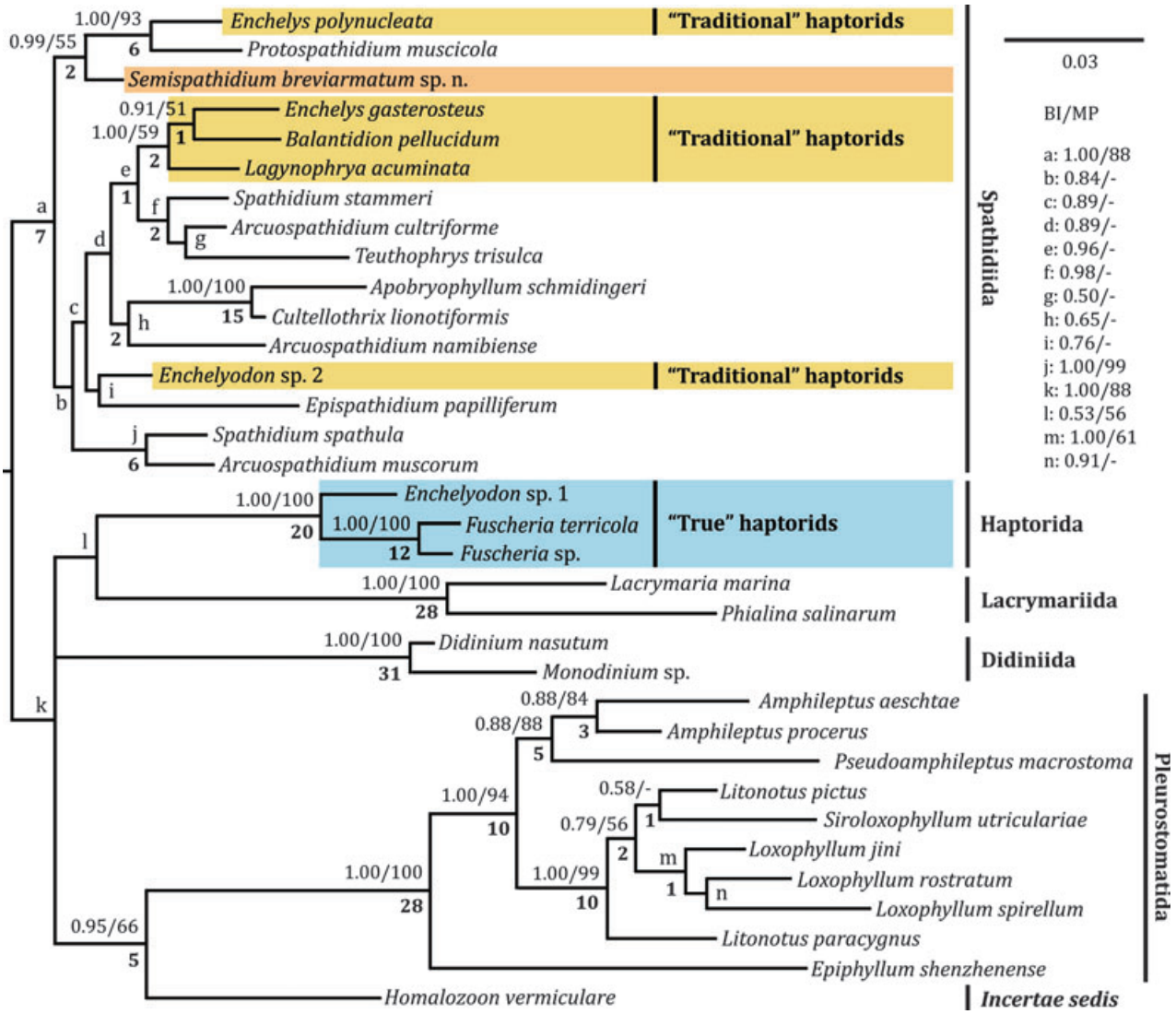

Fig. 9 Phylogenetic analysis of the combined molecular and morphological dataset comprising 34 haptorian taxa and 1556 characters. The tree was constructed with Bayesian inference using mixed models and with the maximum parsimony analysis implemented in PAUP*. Nodal support is indicated by posterior probabilities for Bayesian inference (BI) and the bootstrap values for the maximum parsimony (MP) analysis shown above the nodes. Bremer indices are provided in bold face below the nodes. A dash indicates MP bootstraps below 50%. The scale bar indicates the fraction of substitutions per site.

associated with fine nematodesmata, forming distinct bundles (Figs 1D, E, F, 2B and 4H, I).

Observations on a Botswanan population. In Botswana, we found a population that matches rather well the type population of *Semispathidium breviarmatum* sp. n. in body and extrusome shape as well as in the nuclear and contractile vacuole pattern. On the other hand, both populations slightly deviate from each other in the shape of the oral bulge, which is circular in the Botswanan cells, while broadly elliptical in the type specimens. Moreover, the Botswanan population displays a slightly smaller body (200 × 40 μm vs. 220–490 × 40–90 μm) and slightly shorter oral bulge extrusomes (4–5 × 1 μm vs. 5–7 × 1–1.3 μm) (Fig. 6A–E).

Resting cyst (type population). Cysts *in vivo* colourless, 61–72 μm in diameter, on average 66 μm (n = 3); without escape apparatus. Cyst wall conspicuous because rugose, that is, with irregularly arranged, longitudinally extending vermiform strands appearing 1–2 μm high in optical sections of the cyst; composed of two distinct, refractive layers separated by a sheet of lower refractivity; external and internal refractive layers each about 1 μm thick; covered by a mucous layer

strongly attaching cysts to microscope slide. Cytoplasm finely granulated in periphery; central area packed with innumerable 1–4-μm-sized globules and the oblong macronucleus. Contractile vacuole, extrusomes, cortical granules and cilia not recognizable (Figs 1G, H and 3G, J–L).

Occurrence and ecology. *Semispathidium breviarmatum* sp. n. has been discovered in the Republic of South Africa, that is, in a soil sample from the floodplain of the Matjulu River in the surroundings of the Berg-en-dal Lodge. The Matjulu River is a small tributary to the large Crocodile River at the southern border of the Krüger National Park. The wet soil was collected from the upper 10 cm together with some plant litter and grass roots.

A second population of *S. breviarmatum* has been found in a soil sample from the green river bed of the Thamalakene River near to the town of Maun in Botswana. The wet, sandy and loamy soil was slightly acidic (pH 5.3 in water), black (dark grey when dried) and overgrown with grass because the sample was collected in the dry season.

Cladistic analyses

Out of 27 characters used in the PAUP* analyses, 24 were parsimony informative. The 50% majority-rule consensus tree generated by a weighted approach in the maximum parsimony framework and the 50% majority-rule consensus tree computed with MrBayes had almost identical topology. Thus, we present here the weighted MP tree annotating the posterior probabilities from Bayesian inference (Fig. 7).

Both maximum parsimony and Bayesian inference depicted the orders Lacrymariida, Didiniida and Pleurostomatida as monophyletic each. However, members of the orders Haptorida and Spathidiida did not form monophyletic groups. *Semispathidium breviarmatum* sp. n. was placed in a basal polytomy along with 'true' haptorids (*Enchelyodon* sp. 1 and *Fuscheria* spp.), 'traditional' haptorids (i.e. *Balantidion pellucidum*, *Enchelyodon* sp. 2, *Enchelys* spp. and *Lagynophrya acuminata*), the core spathidiids (i.e. *Spathidium* spp., *Epispathidium papilliferum*, *Arcuospathidium* spp., *Cultellothrix lionotiformis* and *Apobryophyllum schmidingeri*), the didiniids and the lacrymariids (Fig. 7).

Molecular phylogenetic analyses

The overall topology of all trees was identical, but trees inferred from G-block alignment showed a slightly higher statistical support in some nodes than those inferred from Guidance alignment. Therefore, we present here only the results obtained from the former alignment.

All analyses consistently placed *Semispathidium breviarmatum* sp. n. within the order Spathidiida, which was strongly supported by Bayesian inference with a posterior probability of 1.00, moderately supported by the decay analysis with a Bremer index of three and only poorly supported by the 61% ML and 67% MP bootstraps (Fig. 8). In accordance with the cladistic morphological analyses, *S. breviarmatum* was placed in the basal polytomy of the order Spathidiida in the MP tree. However, in the Bayesian and ML trees, *S. breviarmatum* formed a very poorly supported clade comprising *Enchelys polynucleata* and *Protospathidium muscicola*.

All statistical topology tests firmly excluded any closer relationship of *S. breviarmatum* with *Enchelyodon* spp. mostly at the conservative significance level of 0.01 (Table 4). Further, these tests showed that even *Enchelyodon* spp. do not form a monophylum and the *Enchelyodon*-like ciliary pattern evolved very likely convergently in the spathidiid and the haptorid lineages.

Combined analyses

The combined analyses of the macronuclear 18S rRNA gene (G-blocks alignment) and 27 morphological characters resulted in a matrix of 34 taxa and 1556 characters of

Table 4 Log-likelihoods and *P*-values of the AU (approximately unbiased), the WSH (weighted Shimodaira–Hasegawa) and the WKH (weighted Kishino–Hasegawa) tests for tree comparisons considering different topological scenarios and alignment masking methods

Topology	Alignment masking method	Log likelihood (–ln L)	Difference to best tree (–ln L)	AU	WSH	WKH	Conclusion
Best maximum likelihood tree (unconstrained)	G-blocks	7594.6384	–	0.841	0.983	0.808	–
	Guidance	7505.4270	–	0.889	0.990	0.829	–
Monophyly of *Enchelyodon* spp.	G-blocks	7730.4589	135.82	**3e–005**	**0.000**	**0.000**	**Rejected**
	Guidance	7639.4997	134.07	**2e–005**	**0.000**	**0.000**	**Rejected**
Sister relationship of *Enchelyodon* sp. 1 and *Semispathidium breviarmatum* sp. n.	G-blocks	7737.4437	142.81	**5e–046**	**0.000**	**0.000**	**Rejected**
	Guidance	7645.9351	140.51	**1e–004**	**0.000**	**0.000**	**Rejected**
Sister relationship of *Enchelyodon* sp. 2 and *Semispathidium breviarmatum* sp. n.	G-blocks	7625.5253	30.89	**0.004**	**0.030**	**0.014**	**Rejected**
	Guidance	7534.7863	29.36	**0.007**	**0.045**	**0.021**	**Rejected**
Monophyly of *Enchelyodon* spp. and *Semispathidium breviarmatum* sp. n.	G-blocks	7739.9001	145.26	**9e–055**	**0.000**	**0.000**	**Rejected**
	Guidance	7648.7428	143.32	**2e–006**	**0.000**	**0.000**	**Rejected**

Significant differences (*P*-value <0.05) between the best unconstrained and constrained topologies are in bold.

which 258 were parsimony informative. The Bayesian and MP analyses consistently revealed the monophylies of all haptorian orders recognized and defined by Vd'ačný *et al.* (2011a). Support values were very strong for all ordinal-level nodes. Specifically, posterior probabilities (PP) were constantly 1.00, MP bootstraps ranged between 88% and 100%, and Bremer support (BS) varied from 7 to 31 (Fig. 9).

Semispathidium breviarmatum sp. n. nested within the order Spathidiida (1.00 PP, 88% MP, BS 7), forming a clade together with *Protospathidium muscicola* and *Enchelys polynucleata* (0.99 PP, 55% MP, BS 2). This clade was classified as sister to a big, poorly supported cluster comprising the core spathidiids and the majority of 'traditional' haptorids. No closer relationship between *S. breviarmatum* and *Enchelyodon* spp. was revealed in the combined analyses. *Enchelyodon* spp. were again depicted as polyphyletic since *Enchelyodon* sp. 1 clustered within the order Haptorida as expected according to the traditional classifications while *Enchelyodon* sp. 2 nested within the order Spathidiida. This indicates that *Enchelyodon*-like morphology evolved very likely convergently among these two taxa (Fig. 9).

Discussion

Comparison of the new species with congeners

Like the congeners, *Semispathidium breviarmatum* sp. n. exhibits a cylindroidal body and a *Spathidium*-like ciliary pattern, that is, the somatic kineties are anteriorly curved dorsally on the right side of the body, while ventrally on its left side. *Semispathidium breviarmatum* differs from all congeners by the higher number of the ciliary rows (on average 34 vs. on average less than 21) and by the shape of the extrusomes (narrowly to very narrowly ovate vs. obclavate, very narrowly fusiform or filiform). It is important to note that the shape and size of the extrusomes are of a high alpha-taxonomic importance in predatory ciliates because they are used to overwhelm and kill the prey (e.g. Foissner & Xu 2007; Lynn 2008; Vd'ačný & Foissner 2012). Indeed, all *Semispathidium* species can be clearly separated from each other by the extrusome morphology and arrangement, which indicates different preying strategies (Foissner *et al.* 2010). Moreover, *S. breviarmatum* is distinguished from *S. enchelyodontides*, *S. fraterculum* and *S. pulchrum* by the macronuclear pattern: elongate ellipsoidal in *S. breviarmatum*, while fragmented into about 21 nodules in *S. enchelyodontides* (Foissner *et al.* 2002) or forming a nodulated strand in *S. fraterculum* and *S. pulchrum* (Foissner *et al.* 2010). On the other hand, *S. armatum* strongly resembles *S. breviarmatum* in the macronuclear pattern, but distinctly differs from it by the shape of the extrusomes (obclavate with rod-shaped anterior process vs. narrowly to very narrowly ovate) and by the number of the ciliary rows (20–23 vs. 31–37).

Phylogenetic position of Semispathidium

Due to the composite enchelyodonid/spathidiid morphology, the phylogenetic position of *Semispathidium* among the haptorians has been controversial since its discovery by Foissner *et al.* (2002). With respect to the general appearance, *Semispathidium* resembles typical members of the genus *Enchelyodon* in having a cylindroidal body and a more or less discoidal oral bulge, while the course of the ciliary rows resembles *Spathidium* in that the somatic kineties are curved anteriorly (Foissner *et al.* 2002, 2010; Foissner & Xu 2007). Whether *Semispathidium* is more closely related to *Enchelyodon* or *Spathidium* has been not solved by 18S rRNA gene phylogenies, and only Bayesian inference analyses supported significantly its spathidiid origin (Vd'ačný *et al.* 2011a). Now, the combined analyses of the molecular and morphological data sets enhanced the inherent phylogenetic signal, clearly showing that *Semispathidium* belongs to the order Spathidiida. However, *Semispathidium* is nested outside the core spathidiid cluster (Fig. 9), corroborating the assumption of Foissner *et al.* (2002) that *Semispathidium* is far from ordinary *Spathidium* species, representing a divergent spathidiid evolutionary lineage. Our combined analyses further suggest that *Semispathidium* could represent a basal spathidiid branch that may be related to *Protospathidium* and *Enchelys*. Members of these three genera typically exhibit a cylindroidal to bursiform body with more or less discoidal oral bulge, causing the *Enchelyodon*-like appearance. However, *Protospathidium* is clearly separated from *Semispathidium* by the fragmented circumoral kinety, and *Enchelys* differs from *Semispathidium* by the lack of the circumoral kinety (Fig. 10). On the other hand, a closer phylogenetic relationship between *Semispathidium* and *Enchelyodon* spp. has been firmly excluded by all statistical tree topology tests, usually, at the conservative significance level of 0.01 (Table 4).

However, the discussion about the phylogenetic position of *Semispathidium* becomes much more complex when we consider that (i) 'congeneric' species of *Enchelyodon* and *Spathidium* do not form a monophyletic group each (Vd'ačný *et al.* 2011a; present study); (ii) no type species has been fixed for the genus *Enchelyodon* [for details, see Aescht (2001)]; and (iii) the type species of the genera *Spathidium* (i.e. *S. hyalinum*) and *Semispathidium* (i.e. *S. enchelyodontides*) have not yet been analysed molecular biologically. Type species are very important because they define nominal genera according to the principle of typification [Article 61 of the ICZN [International Commission on Zoological Nomenclature] (1999)]. Thus, as long as the placement of type species in a

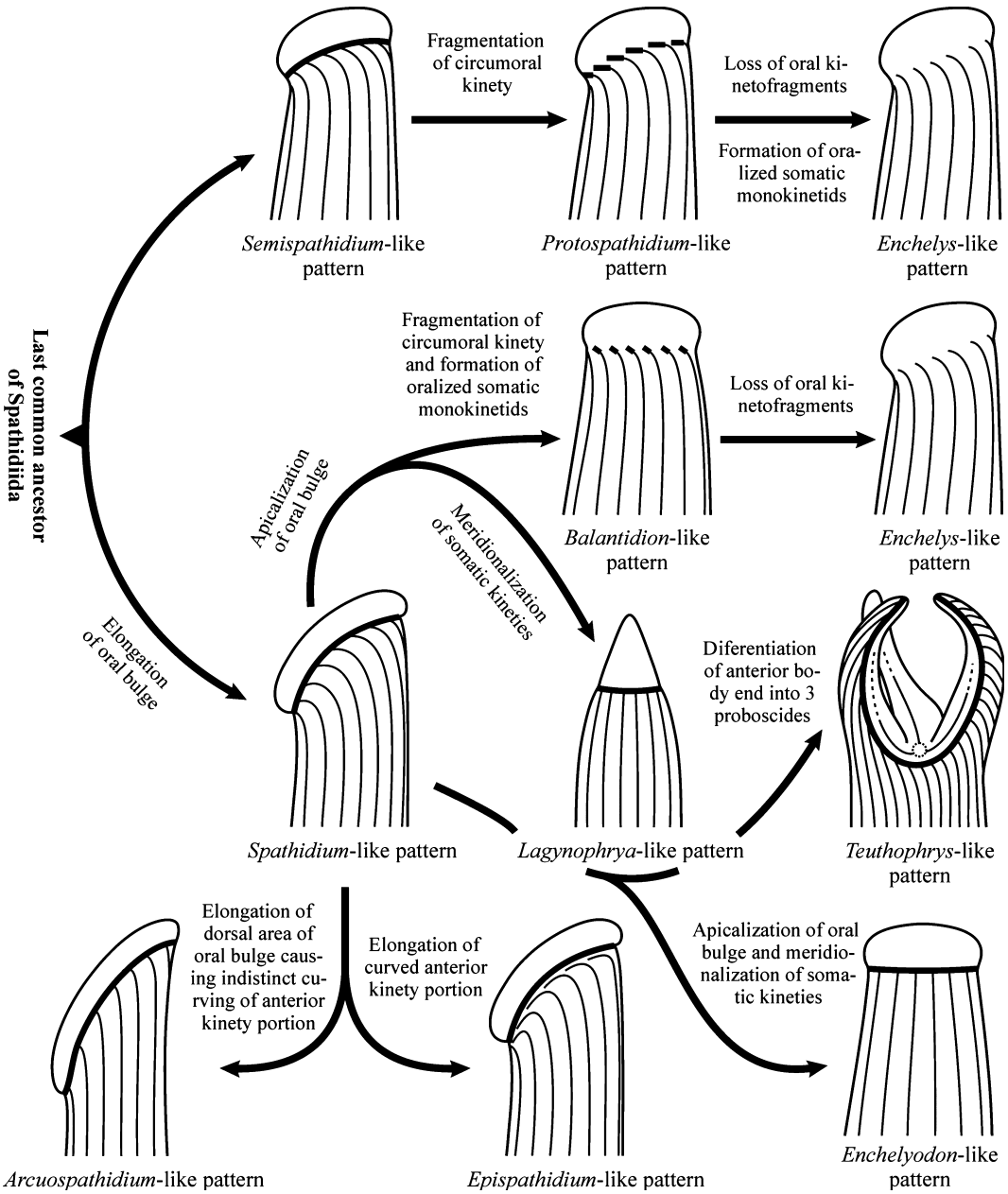

Fig. 10 Hypothesis for the evolution of the oral ciliary patterns in spathidiid ciliates based on the morphology and the present phylogenetic analyses.

phylogenetic framework is not known, the relationships between genera and their species remain somewhat uncertain. Therefore, fixation of type species for *Enchelyodon* and sequencing of type species of all three genera under discussion are needed to obtain a more objective picture about their phylogenetic positions. Nevertheless, the morphological and molecular data available from 34 haptorian taxa indicate that *Semispathidium breviarmatum* represents a basal spathidiid lineage that is more closely related to *Protospathidium musicola*, which is the type species of *Protospathidium*, than to any sequenced species of the genera *Enchelyodon* or *Spathidium*.

Reconstruction of the last common ancestor of the Spathidiida

The likelihood method and the Markov k-state 1-parameter model suggest that the last common ancestor (LCA) of the order Spathidiida had the following ground pattern

© 2013 The Norwegian Academy of Science and Letters, **42**, 5, September 2013, pp 529–549

(proportional likelihoods for the following characters ranged from 0.9946 to 0.9999): (i) a bursiform to cylindroidal body; (ii) a single terminal contractile vacuole; (iii) a three-rowed dorsal brush located on dorsal side; and (iv) anteriorly curved ciliary rows abutting on a continuous dikinetidal circumoral kinety. Only two features will be discussed in a deeper detail, viz. body shape and the oral ciliary pattern, because the other characters were recently treated by Vd'ačný *et al.* (2010, 2011a).

Body shape. Two basic morphologies come into question with respect to the LCA of the Spathidiida: (i) a bursiform to cylindroidal or (ii) a spatulate cytoarchitecture. The majority of species in the spathidiid cluster (i.e. *Balantidion pellucidum*, *Enchelyodon* sp. 2, *Enchelys gasterosteus*, *E. polynucleata*, *Protospathidium muscicola* and *Semispathidium breviarmatum*) displays a bursiform to cylindroidal body like all members of the order Haptorida do (represented here by *Enchelyodon* sp. 1 and *Fuscheria* spp.). On the other hand, only some core spathidiids (e.g. *Spathidium spathula* and *Epispathidium papilliferum*) exhibit the typical spatulate body. According to the likelihood analysis, the LCA of the Spathidiida had, much more likely, a bursiform to cylindroidal body (proportional likelihood 0.9997) than a spatulate one (proportional likelihood 0.0001). The same applies to the morphology of the LCA of the subclass Haptoria, as the proportional likelihood for the bursiform to cylindroidal body is approximately 0.9956. Thus, this body shape is very likely a plesiomorphic feature inherited from the LCA of the Haptoria, and hence, it is not a reliable trait for inferring their phylogenetic relationships.

Oral ciliary pattern. As concerns the oral ciliary pattern of the LCA of the Spathidiida, again two possibilities come into question: (i) an enchelyodonid pattern in which the ciliary rows extend meridionally throughout and thus do not curve anteriorly and (ii) a spathidiid pattern in which the ciliary rows are curved anteriorly. The former pattern is a property of all 'true' haptorids and two fairly distant 'traditional' haptorids (*Enchelyodon* sp. 2 and *Lagynophrya acuminata*), while all other taxa in the spathidiid cluster, including the basal lineages, exhibit the latter pattern (Fig. 10). Therefore, the most parsimonious solution is to assume that the curved anterior ends of somatic kineties were already present in the LCA of the order Spathidiida. This is strongly corroborated by the likelihood analysis of the ancestral character states with a proportional likelihood of 0.9946. However, according to the likelihood analyses, the ciliary rows could be curved anteriorly already in the LCA of the subclass Haptoria, thought with an insignificant proportional likelihood of 0.6805. Thus, it cannot be unambiguously decided whether anteriorly curved ciliary rows evolved independently in the Spathidiida and Didiniida or both groups inherited them from the LCA of the Haptoria. Anyhow, the spathidiid oral ciliary pattern seems to be, at the present state of knowledge, the best morphological feature separating the Spathidiida from the Haptorida. However, molecular data are necessary for a reliable classification because an enchelyodonid-like ciliary pattern, an important feature of the Haptorida, evolved convergently at least two times independently within the core spathidiid cluster, viz. in *Enchelyodon* sp. 2 and *Lagynophrya acuminata* (Fig. 10).

Conclusions

Our phylogenetic analyses show the following:

1. The genus *Semispathidium* is classified within the order Spathidiida and any closer relationship with *Enchelyodon* spp. can be excluded at the present state of knowledge;
2. *Semispathidium* represents a basal spathidiid lineage as it branches off first within the spathidiid clade in 18S rRNA gene and in combined phylogenies. This is also supported by the likelihood analysis of character evolution in which the *Semispathidium* morphology remained virtually unchanged from that of the last common ancestor of the order Spathidiida;
3. A bursiform or cylindroidal body shape is very likely a feature inherited from the last common ancestor of the subclass Haptoria;
4. The spathidiid oral ciliary pattern was either a property of the last common ancestor of the subclass Haptoria or evolved independently in the orders Spathidiida and Didiniida;
5. The enchelyodonid oral ciliary pattern is a typical feature of the order Haptorida, but evolved at least two times convergently also within the spathidiid cluster, viz. in *Enchelyodon* sp. 2 and in *Lagynophrya acuminata*.

Acknowledgements

Financial support was provided by the Austrian Science Foundation (FWF Projects P-19699-B17 and P-20360-B17 to Wilhelm Foissner) and the Slovak Scientific Grant Agency (VEGA Projects 1/0248/13 and 1/0600/11 to Peter Vd'ačný). We are grateful to two anonymous reviewers for their thoughtful comments that led to improvements in the manuscript. The technical assistance of Mag. Gudrun Fuß, Mag. Barbara Harl, Robert Schörghofer and Mgr. Marek Vd'ačný is greatly appreciated.

References

Aescht, E. (2001). Catalogue of the generic names of ciliates (Protozoa, Ciliophora). *Denisia*, *1*, 1–350.

Castresana, J. (2000). Selection of conserved blocks from multiple alignments for their use in phylogenetic analysis. *Molecular Biology and Evolution*, *17*, 540–552.

Claparède, É. & Lachmann, J. (1859). Études sur les infusoires et les rhizopodes. *Mémoires de l'Institut National Genevois*, *6*, 261–482.

Corliss, J. O. (1979). *The Ciliated Protozoa. Characterization, Classification, and Guide to the Literature*. 2nd edn. Oxford, New York, Toronto, Sydney, Paris, Frankfurt: Pergamon Press.

Dragesco, J. & Dragesco-Kernéis, A. (1979). Cilies muscicoles nouveaux ou peu connus. *Acta Protozoologica*, *18*, 401–416.

Dujardin, F. (1841). *Histoire Naturelle des Zoophytes. Infusoires, Comprenant la Physiologie et la Classification de ces Animaux, et la Maniére de les Étudier a l'aide du Microscope*. Paris: Librairie Encyclopédique de Roret.

Foissner, W. (1983). Morphologie und Infraciliatur zweier ectocommensaler Ciliaten (Protozoa: Ciliophora) von *Cyprinus carpio* L. (Pisces: Cypriniformes): *Heteropolaria lwoffi* (Fauré-Fremiet, 1943) (Peritrichida: Epistylididae) und ihr Predator *Pseudoamphileptus macrostoma* (Chen, 1955) nov. gen. (Pleurostomatida: Amphileptidae). *Zoologische Jahrbücher Systematik*, *110*, 399–418.

Foissner, W. (1984). Infraciliatur, Silberliniensystem und Biometrie einiger neuer und wenig bekannter terrestrischer, limnischer und mariner Ciliaten (Protozoa: Ciliophora) aus den Klassen Kinetofragminophora, Colpodea und Polyhymenophora. *Stapfia*, *12*, 1–165.

Foissner, W. (1991). Basic light and scanning electron microscopic methods for taxonomic studies of ciliated protozoa. *European Journal of Protistology*, *27*, 313–330.

Foissner, W. & Al-Rasheid, K. (2007). Notes on soil ciliates (Protozoa, Ciliophora) from the Netherlands, with description of *Keronopsis schminkei* nov. spec. and *Apobryophyllum schmidingeri* nov. spec. *Acta Protozoologica*, *46*, 201–220.

Foissner, W. & Foissner, I. (1985). Oral monokinetids in the free-living haptorid ciliate *Enchelydium polynucleatum* (Ciliophora, Enchelyidae): ultrastructural evidence and phylogenetic implications. *Journal of Protozoology*, *32*, 712–722.

Foissner, W. & Foissner, I. (1988). The fine structure of *Fuscheria terricola* Berger *et al*., 1983 and a proposed new classification of the subclass Haptoria Corliss, 1974 (Ciliophora, Litostomatea). *Archiv für Protistenkunde*, *135*, 213–235.

Foissner, W. & Leipe, D. (1995). Morphology and ecology of *Siroloxophyllum utriculariae* (Penard, 1922) n. g., n. comb. (Ciliophora, Pleurostomatida) and an improved classification of pleurostomatid ciliates. *Journal of Eukaryotic Microbiology*, *42*, 476–490.

Foissner, W. & Xu, K. (2007). Monograph of the Spathidiida (Ciliophora, Haptoria). Vol. I: Protospathidiidae, Arcuospathidiidae, Apertospathulidae. *Monographiae Biologicae*, *81*, 1–485.

Foissner, W., Berger, H., Blatterer, H. & Kohmann, F. (1995). Taxonomische und ökologische Revision der Ciliaten des Saprobiensystems – Band IV: Gymnostomatea, *Loxodes*, Suctoria. *Informationsberichte des Bayerischen Landesamtes für Wasserwirtschaft*, *1/95*, 1–540.

Foissner, W., Berger, H. & Schaumburg, J. (1999). Identification and ecology of limnetic plankton ciliates. *Informationsberichte des Bayerischen Landesamtes für Wasserwirtschaft*, *3/99*, 1–793.

Foissner, W., Agatha, S. & Berger, H. (2002). Soil ciliates (Protozoa, Ciliophora) from Namibia (Southwest Africa), with emphasis on two contrasting environments, the Etosha Region and the Namib Desert. *Denisia*, *5*, 1–1459.

Foissner, W., Hess, S. & Al-Rasheid, K. (2010). Two vicariant *Semispathidium* species from tropical Africa and central Europe: *S. fraterculum* nov. spec. and *S. pulchrum* nov. spec. (Ciliophora, Haptorida). *European Journal of Protistology*, *46*, 61–73.

Gao, S., Song, W., Ma, H., Clamp, J. C., Yi, Z., Al-Rasheid, K. A. S., Chen, Z. & Lin, X. (2008). Phylogeny of six genera of the subclass Haptoria (Ciliophora, Litostomatea) inferred from sequences of the gene coding for small subunit ribosomal RNA. *Journal of Eukaryotic Microbiology*, *55*, 562–566.

Guindon, S. & Gascuel, O. (2003). A simple, fast, accurate algorithm to estimate large phylogenies by maximum likelihood. *Systems Biology*, *52*, 696–704.

Hill, J. (1752). *A General Natural History: Or New and Accurate Descriptions of the Animals, Vegetables and Minerals of the Various Parts of the World; with Their Virtues and Uses, in Medicine and Mechanics: Illustrated by a General Review of the Knowledge of the Ancients; and the Improvements and Discoveries of Later Ages in These Studies*. London: Osborne.

ICZN [International Commission on Zoological Nomenclature] (1999). *International Code of Zoological Nomenclature*. 4th edn. London: The International Trust for Zoological Nomenclature.

Kahl, A. (1930a). Neue und ergänzende Beobachtungen holotricher Infusorien. II. *Archiv für Protistenkunde*, *70*, 313–416.

Kahl, A. (1930b). Urtiere oder Protozoa I: Wimpertiere oder Ciliata (Infusoria) 1. Allgemeiner Teil und Prostomata. *Die Tierwelt Deutschlands*, *18*, 1–180.

Kahl, A. (1931). Urtiere oder Protozoa I: Wimpertiere oder Ciliata (Infusoria) 2. Holotricha außer den im 1. Teil behandelten Prostomata. *Die Tierwelt Deutschlands*, *21*, 181–398.

Katoh, K. & Toh, H. (2008). Recent developments in the MAFFT multiple sequence alignment program. *Briefings in Bioinformatics*, *9*, 286–298.

Kim, S.-J. & Min, G.-S. (2009). Taxonomic study of poorly-known marine pleurostomatid ciliates of *Litonotus paracygnus* and *L. pictus* (Ciliophora: Pleurostomatida) from Korea. *Korean Journal of Systematic Zoology*, *25*, 167–178.

Kück, P., Mayer, C., Wägele, J.-W. & Misof, B. (2012). Long branch effects distort maximum likelihood phylogenies in simulations despite selection of the correct model. *PLoS ONE*, 7, e36593. (doi:10.1371/journal.pone.0036593).

Lin, X., Song, W., Wilbert, N. & Warren, A. (2005). Two new marine pleurostomatid ciliates from China, *Loxophyllum jini* and *L. qiuianum* (Ciliophora: Pleurostomatida). *Acta Protozoologica*, *44*, 147–157.

Lin, X., Song, W. & Li, J. (2007). *Amphileptus aeschtae* nov. spec. and *Amphileptus eigneri* nov. spec. (Ciliophora, Pleurostomatida), two new marine pleurostomatid ciliates from China. *European Journal of Protistology*, *43*, 77–86.

Lin, X., Al-Rasheid, K. A. S., Al-Quraishy, S. A., Al-Farraj, S. A. & Song, W. (2008). Identification of three highly confused marine *Loxophyllum* (Ciliophora: Pleurostomatida) with a key to seven congeners from the China Sea. *Journal of Eukaryotic Microbiology*, *55*, 331–342.

Lipscomb, D. L. & Riordan, G. P. (1990). The ultrastructure of *Chaenea teres* and an analysis of the phylogeny of the haptorid ciliates. *Journal of Protozoology*, *37*, 287–300.

Lipscomb, D. L. & Riordan, G. P. (1992). A reexamination of the ultrastructure of *Didinium nasutum* and a reanalysis of the phylogeny of the haptorid ciliates. *Journal of Protozoology*, *39*, 110–121.

Lynn, D. H. (2008). *The Ciliated Protozoa. Characterization, Classification and Guide to the Literature*. 3rd edn. Dordrecht: Springer.

Maddison, W. P. & Maddison, D. R. (2007). Mesquite: a modular system for evolutionary analysis. Version 2.0. Available via http://mesquiteproject.org.

Miller, M. A., Holder, M. T., Vos, R., Midford, P. E., Liebowitz, T., Chan, L., Hoover, P. & Warnow, T. (2009). The CIPRES Portals. Available via http://www.phylo.org/sub_sections/portal.

Müller, O. F. (1773). *Vermium Terrestrium et Fluviatilium, Seu Animalium Infusoriorum, Helminthicorum et Testaceorum, non Marinorum, Succincta Historia*. Havniae & Lipsiae: Heineck & Faber.

Müller, K. (2004). PRAP-computation of Bremer support for large data sets. *Molecular Phylogenetics and Evolution*, *31*, 780–782.

Pagel, M. (1999). The maximum likelihood approach to reconstructing ancestral character states of discrete characters on phylogenies. *Systematic Biology*, *48*, 612–622.

Pan, H., Gao, F., Li, J., Lin, X., Al-Farraj, S. A. & Al-Rasheid, K. A. S. (2010). Morphology and phylogeny of two new pleurostomatid ciliates, *Epiphyllum shenzhenense* n. sp. and *Loxophyllum spirellum* n. sp. (Protozoa, Ciliophora) from a mangrove wetland, South China. *Journal of Eukaryotic Microbiology*, *57*, 421–428.

Penn, O., Privman, E., Ashkenazy, H., Landan, G., Graur, D. & Pupko, T. (2010a). Guidance: a web server for assessing alignment confidence scores. *Nucleic Acids Research*, *38*, W23–W28.

Penn, O., Privman, E., Landan, G., Graur, D. & Pupko, T. (2010b). An alignment confidence score capturing robustness to guide-tree uncertainty. *Molecular Biology and Evolution*, *27*, 1759–1767.

Posada, D. (2008). JModelTest: phylogenetic model averaging. *Molecular Biology and Evolution*, *25*, 1253–1256.

Ronquist, F. & Huelsenbeck, J. P. (2003). MrBayes 3: Bayesian phylogenetic inference under mixed models. *Bioinformatics*, *19*, 1572–1574.

Schulter, D., Price, T., Mooers, A. O. & Ludwig, D. (1997). Likelihood of ancestor states in adaptive radiation. *Evolution*, *51*, 1699–1711.

Shimodaira, H. & Hasegawa, M. (2001). Consel: for assessing the confidence of phylogenetic tree selection. *Bioinformatics*, *17*, 1246–1247.

Song, W., Zhao, Y., Xu, K., Hu, X. & Gong, J. (2003). *Pathogenic Protozoa in Mariculture*. Beijing: Science Press.

Stamatakis, A., Hoover, P. & Rougemont, J. (2008). A rapid bootstrap algorithm for the RAxML web-servers. *Systematic Biology*, *75*, 758–771.

Strüder-Kypke, M. C., Wright, A.-D. G., Foissner, W., Chatzinotas, A. & Lynn, D. H. (2006). Molecular phylogeny of litostome ciliates (Ciliophora, Litostomatea) with emphasis on free-living haptorian genera. *Protist*, *157*, 261–278.

Swofford, D. L. (2003). *PAUP*. Phylogenetic Analysis Using Parsimony (*and Other Methods). Ver. 4. [Computer software and manual]*. Sunderland, MA: Sinauer Associates.

Talavera, G. & Castresana, J. (2007). Improvement of phylogenies after removing divergent and ambiguously aligned blocks from protein sequence alignments. *Systematic Biology*, *56*, 564–577.

Vd'ačný, P. & Foissner, W. (2012). Monograph of the dileptids (Protista, Ciliophora, Rhynchostomatia). *Denisia*, *31*, 1–529.

Vd'ačný, P., Orsi, W. & Foissner, W. (2010). Molecular and morphological evidence for a sister group relationship of the classes Armophorea and Litostomatea (Ciliophora, Intramacronucleata, Lamellicorticata infraphyl. nov.), with an account on basal haptorid litostomateans. *European Journal of Protistology*, *46*, 298–309.

Vd'ačný, P., Bourland, W. A., Orsi, W., Epstein, S. S. & Foissner, W. (2011a). Phylogeny and classification of the Litostomatea (Protista, Ciliophora), with emphasis on free-living taxa and the 18S rRNA gene. *Molecular Phylogenetics and Evolution*, *59*, 510–522.

Vd'ačný, P., Orsi, W., Bourland, W. A., Shimano, S., Epstein, S. S. & Foissner, W. (2011b). Morphological and molecular phylogeny of dileptids: resolution at the base of the class Litostomatea (Ciliophora, Intramacronucleata). *European Journal of Protistology*, *47*, 295–313.

Vd'ačný, P., Bourland, W. A., Orsi, W., Epstein, S. S. & Foissner, W. (2012). Genealogical analyses of multiple loci of litostomatean ciliates (Protista, Ciliophora, Litostomatea). *Molecular Phylogenetics and Evolution*, *65*, 397–411.

Wenzel, F. (1959). Ein Beitrag zur Kenntnis der Ciliatengattung *Spathidium* (*S. stammeri* n. sp.). *Zoologischer Anzeiger*, *163*, 209–216.

Williams, D. B., Williams, B. D. & Hogan, B. K. (1981). Ultrastructure of the somatic cortex of the gymnostome ciliate *Spathidium spathula* (O.F.M.). *Journal of Protozoology*, *28*, 90–99.

Zhang, Q., Simpson, A. & Song, W. (2012). Insights into the phylogeny of systematically controversial haptorian ciliates (Ciliophora, Litostomatea) based on multigene analyses. *Proceedings of the Royal Society B, Biological Sciences*, *279*, 2625–2635.